Search for charged massive long-lived particles at $\sqrt{s} = 1.96$ TeV

V.M. Abazov,[32] B. Abbott,[68] B.S. Acharya,[26] M. Adams,[46] T. Adams,[44] G.D. Alexeev,[32] J. Alimena,[70] G. Alkhazov,[36] A. Alton[a],[57] A. Askew,[44] S. Atkins,[55] K. Augsten,[7] C. Avila,[5] F. Badaud,[10] L. Bagby,[45] B. Baldin,[45] D.V. Bandurin,[44] S. Banerjee,[26] E. Barberis,[56] P. Baringer,[53] J.F. Bartlett,[45] U. Bassler,[15] V. Bazterra,[46] A. Bean,[53] M. Begalli,[2] L. Bellantoni,[45] S.B. Beri,[24] G. Bernardi,[14] R. Bernhard,[19] I. Bertram,[39] M. Besançon,[15] R. Beuselinck,[40] P.C. Bhat,[45] S. Bhatia,[59] V. Bhatnagar,[24] G. Blazey,[47] S. Blessing,[44] K. Bloom,[60] A. Boehnlein,[45] D. Boline,[65] E.E. Boos,[34] G. Borissov,[39] A. Brandt,[71] O. Brandt,[20] R. Brock,[58] A. Bross,[45] D. Brown,[14] J. Brown,[14] X.B. Bu,[45] M. Buehler,[45] V. Buescher,[21] V. Bunichev,[34] S. Burdin[b],[39] C.P. Buszello,[38] E. Camacho-Pérez,[29] B.C.K. Casey,[45] H. Castilla-Valdez,[29] S. Caughron,[58] S. Chakrabarti,[65] D. Chakraborty,[47] K.M. Chan,[51] A. Chandra,[73] E. Chapon,[15] G. Chen,[53] S.W. Cho,[28] S. Choi,[28] B. Choudhary,[25] S. Cihangir,[45] D. Claes,[60] J. Clutter,[53] M. Cooke,[45] W.E. Cooper,[45] M. Corcoran,[73] F. Couderc,[15] M.-C. Cousinou,[12] D. Cutts,[70] A. Das,[42] G. Davies,[40] S.J. de Jong,[30,31] E. De La Cruz-Burelo,[29] F. Déliot,[15] R. Demina,[64] D. Denisov,[45] S.P. Denisov,[35] S. Desai,[45] C. Deterre[d],[20] K. DeVaughan,[60] H.T. Diehl,[45] M. Diesburg,[45] P.F. Ding,[41] A. Dominguez,[60] A. Dubey,[25] L.V. Dudko,[34] D. Duggan,[61] A. Duperrin,[12] S. Dutt,[24] A. Dyshkant,[47] M. Eads,[47] D. Edmunds,[58] J. Ellison,[43] V.D. Elvira,[45] Y. Enari,[14] H. Evans,[49] V.N. Evdokimov,[35] G. Facini,[56] L. Feng,[47] T. Ferbel,[64] F. Fiedler,[21] F. Filthaut,[30,31] W. Fisher,[58] H.E. Fisk,[45] M. Fortner,[47] H. Fox,[39] S. Fuess,[45] A. Garcia-Bellido,[64] J.A. García-González,[29] G.A. García-Guerra[c],[29] V. Gavrilov,[33] W. Geng,[12,58] C.E. Gerber,[46] Y. Gershtein,[61] G. Ginther,[45,64] G. Golovanov,[32] P.D. Grannis,[65] S. Greder,[16] H. Greenlee,[45] G. Grenier,[17] Ph. Gris,[10] J.-F. Grivaz,[13] A. Grohsjean[d],[15] S. Grünendahl,[45] M.W. Grünewald,[27] T. Guillemin,[13] G. Gutierrez,[45] P. Gutierrez,[68] J. Haley,[56] L. Han,[4] K. Harder,[41] A. Harel,[64] J.M. Hauptman,[52] J. Hays,[40] T. Head,[41] T. Hebbeker,[18] D. Hedin,[47] H. Hegab,[69] A.P. Heinson,[43] U. Heintz,[70] C. Hensel,[20] I. Heredia-De La Cruz,[29] K. Herner,[57] G. Hesketh[f],[41] M.D. Hildreth,[51] R. Hirosky,[74] T. Hoang,[44] J.D. Hobbs,[65] B. Hoeneisen,[9] J. Hogan,[73] M. Hohlfeld,[21] I. Howley,[71] Z. Hubacek,[7,15] V. Hynek,[7] I. Iashvili,[63] Y. Ilchenko,[72] R. Illingworth,[45] A.S. Ito,[45] S. Jabeen,[70] M. Jaffré,[13] A. Jayasinghe,[68] M.S. Jeong,[28] R. Jesik,[40] P. Jiang,[4] K. Johns,[42] E. Johnson,[58] M. Johnson,[45] A. Jonckheere,[45] P. Jonsson,[40] J. Joshi,[43] A.W. Jung,[45] A. Juste,[37] E. Kajfasz,[12] D. Karmanov,[34] P.A. Kasper,[45] I. Katsanos,[60] R. Kehoe,[72] S. Kermiche,[12] N. Khalatyan,[45] A. Khanov,[69] A. Kharchilava,[63] Y.N. Kharzheev,[32] I. Kiselevich,[33] J.M. Kohli,[24] A.V. Kozelov,[35] J. Kraus,[59] A. Kumar,[63] A. Kupco,[8] T. Kurča,[17] V.A. Kuzmin,[34] S. Lammers,[49] G. Landsberg,[70] P. Lebrun,[17] H.S. Lee,[28] S.W. Lee,[52] W.M. Lee,[44] X. Lei,[42] J. Lellouch,[14] D. Li,[14] H. Li,[74] L. Li,[43] Q.Z. Li,[45] J.K. Lim,[28] D. Lincoln,[45] J. Linnemann,[58] V.V. Lipaev,[35] R. Lipton,[45] H. Liu,[72] Y. Liu,[4] A. Lobodenko,[36] M. Lokajicek,[8] R. Lopes de Sa,[65] R. Luna-Garcia[g],[29] A.L. Lyon,[45] A.K.A. Maciel,[1] R. Magaña-Villalba,[29] S. Malik,[60] V.L. Malyshev,[32] Y. Maravin,[54] J. Martínez-Ortega,[29] R. McCarthy,[65] C.L. McGivern,[41] M.M. Meijer,[30,31] A. Melnitchouk,[45] D. Menezes,[47] P.G. Mercadante,[3] M. Merkin,[34] A. Meyer,[18] J. Meyer,[20] F. Miconi,[16] N.K. Mondal,[26] M. Mulhearn,[74] E. Nagy,[12] M. Naimuddin,[25] M. Narain,[70] R. Nayyar,[42] H.A. Neal,[57] J.P. Negret,[5] P. Neustroev,[36] H.T. Nguyen,[74] T. Nunnemann,[22] J. Orduna,[73] N. Osman,[12] J. Osta,[51] M. Padilla,[43] A. Pal,[71] N. Parashar,[50] V. Parihar,[70] S.K. Park,[28] R. Partridge[e],[70] N. Parua,[49] A. Patwa,[66] B. Penning,[45] M. Perfilov,[34] Y. Peters,[20] K. Petridis,[41] G. Petrillo,[64] P. Pétroff,[13] M.-A. Pleier,[66] P.L.M. Podesta-Lerma[h],[29] V.M. Podstavkov,[45] A.V. Popov,[35] M. Prewitt,[73] D. Price,[49] N. Prokopenko,[35] J. Qian,[57] A. Quadt,[20] B. Quinn,[59] M.S. Rangel,[1] K. Ranjan,[25] P.N. Ratoff,[39] I. Razumov,[35] P. Renkel,[72] I. Ripp-Baudot,[16] F. Rizatdinova,[69] M. Rominsky,[45] A. Ross,[39] C. Royon,[15] P. Rubinov,[45] R. Ruchti,[51] G. Sajot,[11] P. Salcido,[47] A. Sánchez-Hernández,[29] M.P. Sanders,[22] A.S. Santos[i],[1] G. Savage,[45] L. Sawyer,[55] T. Scanlon,[40] R.D. Schamberger,[65] Y. Scheglov,[36] H. Schellman,[48] C. Schwanenberger,[41] R. Schwienhorst,[58] J. Sekaric,[53] H. Severini,[68] E. Shabalina,[20] V. Shary,[15] S. Shaw,[58] A.A. Shchukin,[35] R.K. Shivpuri,[25] V. Simak,[7] P. Skubic,[68] P. Slattery,[64] D. Smirnov,[51] K.J. Smith,[63] G.R. Snow,[60] J. Snow,[67] S. Snyder,[66] S. Söldner-Rembold,[41] L. Sonnenschein,[18] K. Soustruznik,[6] J. Stark,[11] D.A. Stoyanova,[35] M. Strauss,[68] L. Suter,[41] P. Svoisky,[68] M. Titov,[15] V.V. Tokmenin,[32] Y.-T. Tsai,[64] D. Tsybychev,[65] B. Tuchming,[15] C. Tully,[62] L. Uvarov,[36] S. Uvarov,[36] S. Uzunyan,[47] R. Van Kooten,[49] W.M. van Leeuwen,[30] N. Varelas,[46] E.W. Varnes,[42] I.A. Vasilyev,[35] P. Verdier,[17] A.Y. Verkheev,[32] L.S. Vertogradov,[32] M. Verzocchi,[45] M. Vesterinen,[41] D. Vilanova,[15] P. Vokac,[7] H.D. Wahl,[44] M.H.L.S. Wang,[45] J. Warchol,[51] G. Watts,[75] M. Wayne,[51] J. Weichert,[21] L. Welty-Rieger,[48] A. White,[71] D. Wicke,[23] M.R.J. Williams,[39] G.W. Wilson,[53] M. Wobisch,[55] D.R. Wood,[56] T.R. Wyatt,[41] Y. Xie,[45] R. Yamada,[45] S. Yang,[4] T. Yasuda,[45] Y.A. Yatsunenko,[32] W. Ye,[65] Z. Ye,[45] H. Yin,[45] K. Yip,[66] S.W. Youn,[45] J.M. Yu,[57] J. Zennamo,[63] T.G. Zhao,[41] B. Zhou,[57] J. Zhu,[57] M. Zielinski,[64] D. Zieminska,[49] and L. Zivkovic[14]

(The D0 Collaboration*)

[1]LAFEX, Centro Brasileiro de Pesquisas Físicas, Rio de Janeiro, Brazil
[2]Universidade do Estado do Rio de Janeiro, Rio de Janeiro, Brazil
[3]Universidade Federal do ABC, Santo André, Brazil
[4]University of Science and Technology of China, Hefei, People's Republic of China
[5]Universidad de los Andes, Bogotá, Colombia
[6]Charles University, Faculty of Mathematics and Physics, Center for Particle Physics, Prague, Czech Republic
[7]Czech Technical University in Prague, Prague, Czech Republic
[8]Center for Particle Physics, Institute of Physics, Academy of Sciences of the Czech Republic, Prague, Czech Republic
[9]Universidad San Francisco de Quito, Quito, Ecuador
[10]LPC, Université Blaise Pascal, CNRS/IN2P3, Clermont, France
[11]LPSC, Université Joseph Fourier Grenoble 1, CNRS/IN2P3, Institut National Polytechnique de Grenoble, Grenoble, France
[12]CPPM, Aix-Marseille Université, CNRS/IN2P3, Marseille, France
[13]LAL, Université Paris-Sud, CNRS/IN2P3, Orsay, France
[14]LPNHE, Universités Paris VI and VII, CNRS/IN2P3, Paris, France
[15]CEA, Irfu, SPP, Saclay, France
[16]IPHC, Université de Strasbourg, CNRS/IN2P3, Strasbourg, France
[17]IPNL, Université Lyon 1, CNRS/IN2P3, Villeurbanne, France and Université de Lyon, Lyon, France
[18]III. Physikalisches Institut A, RWTH Aachen University, Aachen, Germany
[19]Physikalisches Institut, Universität Freiburg, Freiburg, Germany
[20]II. Physikalisches Institut, Georg-August-Universität Göttingen, Göttingen, Germany
[21]Institut für Physik, Universität Mainz, Mainz, Germany
[22]Ludwig-Maximilians-Universität München, München, Germany
[23]Fachbereich Physik, Bergische Universität Wuppertal, Wuppertal, Germany
[24]Panjab University, Chandigarh, India
[25]Delhi University, Delhi, India
[26]Tata Institute of Fundamental Research, Mumbai, India
[27]University College Dublin, Dublin, Ireland
[28]Korea Detector Laboratory, Korea University, Seoul, Korea
[29]CINVESTAV, Mexico City, Mexico
[30]Nikhef, Science Park, Amsterdam, the Netherlands
[31]Radboud University Nijmegen, Nijmegen, the Netherlands
[32]Joint Institute for Nuclear Research, Dubna, Russia
[33]Institute for Theoretical and Experimental Physics, Moscow, Russia
[34]Moscow State University, Moscow, Russia
[35]Institute for High Energy Physics, Protvino, Russia
[36]Petersburg Nuclear Physics Institute, St. Petersburg, Russia
[37]Institució Catalana de Recerca i Estudis Avançats (ICREA) and Institut de Física d'Altes Energies (IFAE), Barcelona, Spain
[38]Uppsala University, Uppsala, Sweden
[39]Lancaster University, Lancaster LA1 4YB, United Kingdom
[40]Imperial College London, London SW7 2AZ, United Kingdom
[41]The University of Manchester, Manchester M13 9PL, United Kingdom
[42]University of Arizona, Tucson, Arizona 85721, USA
[43]University of California Riverside, Riverside, California 92521, USA
[44]Florida State University, Tallahassee, Florida 32306, USA
[45]Fermi National Accelerator Laboratory, Batavia, Illinois 60510, USA
[46]University of Illinois at Chicago, Chicago, Illinois 60607, USA
[47]Northern Illinois University, DeKalb, Illinois 60115, USA
[48]Northwestern University, Evanston, Illinois 60208, USA
[49]Indiana University, Bloomington, Indiana 47405, USA
[50]Purdue University Calumet, Hammond, Indiana 46323, USA
[51]University of Notre Dame, Notre Dame, Indiana 46556, USA
[52]Iowa State University, Ames, Iowa 50011, USA
[53]University of Kansas, Lawrence, Kansas 66045, USA
[54]Kansas State University, Manhattan, Kansas 66506, USA
[55]Louisiana Tech University, Ruston, Louisiana 71272, USA
[56]Northeastern University, Boston, Massachusetts 02115, USA
[57]University of Michigan, Ann Arbor, Michigan 48109, USA
[58]Michigan State University, East Lansing, Michigan 48824, USA
[59]University of Mississippi, University, Mississippi 38677, USA
[60]University of Nebraska, Lincoln, Nebraska 68588, USA
[61]Rutgers University, Piscataway, New Jersey 08855, USA

[62]Princeton University, Princeton, New Jersey 08544, USA
[63]State University of New York, Buffalo, New York 14260, USA
[64]University of Rochester, Rochester, New York 14627, USA
[65]State University of New York, Stony Brook, New York 11794, USA
[66]Brookhaven National Laboratory, Upton, New York 11973, USA
[67]Langston University, Langston, Oklahoma 73050, USA
[68]University of Oklahoma, Norman, Oklahoma 73019, USA
[69]Oklahoma State University, Stillwater, Oklahoma 74078, USA
[70]Brown University, Providence, Rhode Island 02912, USA
[71]University of Texas, Arlington, Texas 76019, USA
[72]Southern Methodist University, Dallas, Texas 75275, USA
[73]Rice University, Houston, Texas 77005, USA
[74]University of Virginia, Charlottesville, Virginia 22904, USA
[75]University of Washington, Seattle, Washington 98195, USA

We present a search for charged massive long-lived particles (CMLLPs) that are pair produced in $p\bar{p}$ collisions at $\sqrt{s} = 1.96$ TeV collected by the D0 experiment at the Fermilab Tevatron collider. Our result is a combination of two searches where either one or both CMLLPs are reconstructed in the detector. We select events with muon-like particles that have both speed and ionization energy loss ($\mathrm{d}E/\mathrm{d}x$) different from muons produced in $p\bar{p}$ collisions. In the absence of evidence for CMLLPs corresponding to 6.3 fb^{-1} of integrated luminosity, we set limits on the CMLLP masses in several supersymmetric (SUSY) models, excluding masses below 278 GeV for long-lived gaugino-like charginos, and masses below 244 GeV for long-lived higgsino-like charginos at the 95% C.L. We also set limits on the cross section for pair production of long-lived scalar tau leptons that range from 0.04 pb to 0.008 pb for scalar tau lepton masses of 100 to 300 GeV.

I. INTRODUCTION

Several extensions of the standard model (SM) including some SUSY models predict the existence of massive long-lived particles (MLLP) [1]. Their existence could explain the origin of dark matter. Primordial lithium abundance is not described by the current model of big bang nucleosynthesis, but it can be satisfactorily explained by the existence of a MLLP that decays during or after big bang nucleosynthesis [2]. MLLPs could have color or electric charge. They appear as R-hadrons (bound states of squarks or gluinos with SM quarks), as sleptons, or as charginos. MLLPs are relatively slow moving at the collision energy of $\sqrt{s} = 1.96$ TeV and for MLLP masses of 100 GeV or greater considered in this article. Charged MLLPs also have large ionization energy loss ($\mathrm{d}E/\mathrm{d}x$) due to their slow speeds. These characteristics are different from other particles studied at high energy colliders, and thus the identification of such particles is simplified by the corresponding small amount of background. We therefore search for charged massive long-lived particles (CMLLPs) at the Tevatron.

Searches for CMLLPs were performed previously by the D0 [3–5], CDF [6, 7], LEP [8], CMS [9], and ATLAS [10] collaborations. We present limits on masses of CMLLPs by combining data from a search for pair produced CMLLPs performed with 1.1 fb^{-1} integrated luminosity [5] with an analysis based on 5.2 fb^{-1} integrated luminosity [11]. The second analysis includes searches for either a pair of CMLLPs or a single CMLLP signature in an event. This article provides greater detail on the analysis and results published in [11].

In this study "long-lived" refers to particles that traverse the entire detector before decaying. Although cosmological observations place severe limits on stable massive particles [1, 12], these limits do not rule out the particles predicted by models studied here. We are sensitive to CMLLPs with lifetimes longer than 25 ns, with best sensitivity for lifetimes longer than 1 μs.

We compare the results with predictions of several SUSY models. Models with gauge-mediated SUSY-breaking (GMSB) always contain a light gravitino/goldstino as the lightest SUSY particle (LSP) [13, 14]. The next-to-lightest SUSY particle (NLSP) could be the lightest scalar tau lepton (stau) or the lightest neutralino, depending on the model parameters [15, 16]. The GMSB parameters assumed in this paper make the stau lepton the NLSP. If stau lepton decays to the gravitino/goldstino are suppressed (the effective coupling to the gravitino/goldstino is a free parameter in the model), then the stau lepton can live long enough to escape the detector and be a candidate CMLLP [17, 18].

Long-lived charginos can occur in models with anomaly mediated SUSY breaking and in SUSY models that do not have gaugino mass unification, provided the difference between the masses of the lightest chargino and the lightest neutralino is less than approximately 150 MeV [19, 20]. The chargino can be mostly higgsino or mostly gaugino. We treat these two cases separately.

*with visitors from [a]Augustana College, Sioux Falls, SD, USA, [b]The University of Liverpool, Liverpool, UK, [c]UPIITA-IPN, Mexico City, Mexico, [d]DESY, Hamburg, Germany, [e]SLAC, Menlo Park, CA, USA, [f]University College London, London, UK, [g]Centro de Investigacion en Computacion - IPN, Mexico City, Mexico, [h]ECFM, Universidad Autonoma de Sinaloa, Culiacán, Mexico and [i]Universidade Estadual Paulista, São Paulo, Brazil.

The analysis strategy is the same as that for the stau lepton search.

In addition, some SUSY models predict long-lived top squark NLSPs that hadronize into mesons and baryons with long enough lifetimes to be CMLLP candidates [21]. Hidden valley models predict scenarios where the top squark acts like the LSP and has a long lifetime [22, 23]. In these models the top squark forms hadrons that are CMLLP candidates. Any SUSY scenario where the top squark is the lightest colored SUSY particle can have a hadron formed with a top squark that is a CMLLP. Colored CMLLPs will hadronize and experience charge exchange during nuclear interactions. This effect is taken into account in the analyses reported here.

A brief description of the D0 detector is given in Sec. II, which is followed in Sec. III by a description of the trigger and the data used. Section IV describes the theory and the signal generation. Section V presents the strategies and techniques used in these analyses. Section VI describes the search for pairs of CMLLPs and Sec. VII the search for single CMLLPs with an integrated luminosity of 5.2 fb^{-1}. "Pair" and "single" refer to the number of detected particles. In the models we consider, CMLLPs are always produced in pairs. Section VIII summarizes the earlier search with an integrated luminosity of 1.1 fb^{-1}. The combined results are presented in Sec. IX. Section X summarizes this study.

II. DETECTOR

Figure 1 shows the details of the D0 detector [24] which consists of three primary systems: a central tracking system, calorimeters, and a muon spectrometer. The polar angle θ is defined such that $\theta = 0$ is the $+z$ direction, which is the direction of the proton beam. The azimuthal angle ϕ is defined such that $\phi = 0$ lies along the horizontal $+x$ axis, pointing outwards from the center of the Tevatron ring and $\phi = \pi/2$ in the $+y$ direction. The pseudorapidity of a particle is defined as $\eta = -\ln[\tan(\theta/2)]$.

The silicon microstrip tracker (SMT) is the innermost part of the tracking system and has a six-barrel longitudinal structure, where each barrel consists of a set of four layers arranged axially around the beampipe to measure the r-ϕ coordinates of charged particles. A new layer of SMT sensors was installed near the beampipe in 2006. The data recorded before this addition are referred to as Run IIa and the subsequent data are referred to as Run IIb. Twelve radial disks, interspersed between the barrel segments, provide position measurement in the r-z and r-ϕ planes. The SMT provides a spatial resolution of approximately 10 μm in r-ϕ and approximately 100 μm in r-z and covers a pseudorapidity range $|\eta| < 3$. The SMT is also used to measure ionization energy loss ($\mathrm{d}E/\mathrm{d}x$) of tracks. The central fiber tracker (CFT) surrounds the SMT and consists of eight concentric carbon fiber barrels holding doublet layers of scintillating fibers (one axial and one small-angle stereo layer) with the outermost barrel covering the region $|\eta| < 1.7$. A superconducting solenoidal magnet surrounds the CFT and provides a uniform 1.9 T axial magnetic field.

A liquid argon/uranium calorimeter measures both electromagnetic and hadronic energy and is housed in three cryostats, with the central calorimeter covering the region $|\eta| < 1.1$ and two end calorimeters covering the region $1.5 < |\eta| < 4.2$. The calorimeter is made of pseudo projective towers consisting of an absorber plate and a signal board. Liquid-argon, the active material of the calorimeter, fills the gap. There are about 10 hadronic interaction lengths in the calorimeter at $\eta = 0$.

The muon system is the outermost part of the D0 detector and covers the region $|\eta| < 2$ [25]. It comprises drift tubes and scintillation counters arranged in three layers (A, B, and C). Between layers A and B, there is magnetized steel (6 interaction lengths at $\eta = 0$) generating a 1.8 T toroidal field. In the central layers ($|\eta| < 1$) multiwire proportional drift tubes (PDT) and in the forward layers ($1 < |\eta| < 2$), mini drift tubes (MDT) are used for tracking. Scintillation counters covering the region ($|\eta| < 2$) are used for triggering on muons.

The PDTs are typically 2.8×5.6 m^2, with cells that are 10 cm in diameter. Typical chambers are built of three or four layers of 24 cell wide planes. Each cell has an anode wire at its center. Vernier cathode pads are located on both sides of the wires to provide information on the hit position along the wire. The chambers are filled with a gas mixture of 84% argon, 8% CF_4, and 8% CH_4 with a drift velocity of approximately 10 cm/μs.

Scintillation counters are installed on the top, the sides and the bottom of the outer layers of the central muon PDTs. They provide a fast signal to associate a muon in a PDT with the appropriate bunch crossing and hence are used in muon triggers. They also help to discriminate against the cosmic ray background and to reject out-of-time particles scattered from accelerator and detector components at high η. The time resolution is approximately 2 ns for A-layer counters and approximately 4 ns for B, and C-layer counters. Detection efficiency is close to 100% in all counters.

In the forward region, MDTs with a drift time of ~ 90 ns provide good coordinate resolution of less than 1 mm, radiation hardness, high segmentation, and low occupancy. Each MDT layer is divided into octants. An MDT consists of eight cells, each with a 9.4×9.4 mm^2 internal cross section and uses a fast gas mixture of CF_4/CH_4 (90%:10%). There are 4214 scintillation counters in the forward region, arranged in three layers (A, B, and C). The segmentation is $4.5^\circ \times 0.12$ (0.07) in $\phi \times \eta$ for the first nine inner (last three) rows of counters. The scintillation counters are 1.3 cm thick with various cross sections ranging from 60×106 cm^2 to 17×24 cm^2. The time resolution is approximately 2 ns and the detection efficiency is above 99.9%. The CMLLPs considered in this analysis would be identified as muons in the D0 detector as they penetrate the material of the calorimeter and the toroid and leave hits in the muon system. An

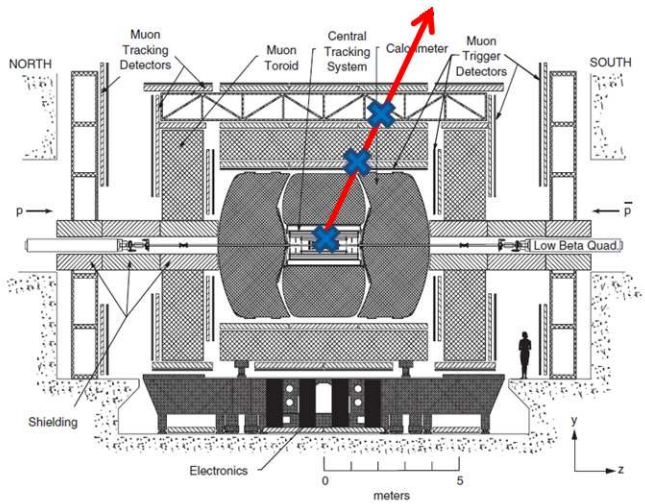

FIG. 1: (color online) Diagram of the D0 detector showing the locations (blue crosses) where a top squark hadron must be measured as charged to be selected as a CMLLP candidate.

accurate measurement of the time of flight (TOF) of a charged particle reaching a scintillation counter is obtained from the position of the counter and the recorded time of the hit. Particle tracks are reconstructed in the muon system using hits from scintillation counters and drift tubes. A muon candidate is qualified as a good muon if it has hits in scintillation counter layers A and either B or C, and multiple drift tube hits in different detector layers. These *local muons* reconstructed by the muon spectrometer are then matched to charged particle tracks in the central tracking system originating at the $p\bar{p}$ interaction vertex. The muon candidate is rejected if no match is found. Otherwise, the measurement of the momentum component transverse to the beam line (p_T) of the muons is taken from the parameters of the central track. To discriminate between muons produced in hadronic decays (which tend to be surrounded by other charged particles and calorimeter energy deposits) and isolated muons, two different isolation quantities are calculated. *Track isolation* is the sum of the p_T of all other tracks in the central tracking system in a cone of radius $\Delta R = \sqrt{(\Delta\eta)^2 + (\Delta\phi)^2} < 0.5$ around the central track matched to the muon. *Calorimeter isolation* is the sum of all energy deposits in the calorimeter in an annulus of $0.1 < \Delta R < 0.4$ around the muon trajectory. Throughout this article, isolated muons will be those with track and calorimeter isolation less than 2.5 GeV each.

III. TRIGGER

The D0 trigger system is designed with three distinct levels with each succeeding level examining fewer events in greater detail so that the final trigger rate is low enough for the data to be recorded without causing excessive dead time. The first stage (L1) comprising a collection of hardware elements that selects events based on features such as momentum, energy and particle type, provides an accept rate of about 2 kHz. In the second stage (L2) microprocessors associated with specific subdetectors provide information to a global processor to construct a trigger decision based on individual objects as well as object correlations. The L2 system has an accept rate of approximately 1 kHz. Candidates accepted by L1 and L2 are sent to the third level (L3) of the trigger system where the data is processed by algorithms on a computing farm to reduce the rate to about 200 Hz. Events that pass all three trigger levels are recorded for offline reconstruction.

As described earlier, the CMLLPs in this study have muon-like signatures with regards to their penetration characteristics in the detector. The p_T threshold of the muon triggering the event varies from 8 GeV to 13 GeV. The earlier analysis performed with an integrated luminosity of 1.1 fb^{-1} from Run IIa searched for a pair of muons in an event using a triggering condition that requires at least two muons to be present in the event (dimuon trigger). In the recent analysis with an integrated luminosity of 5.2 fb^{-1} of Run IIb data, the search is expanded to include events with only one CMLLP candidate. Hence, triggering conditions requiring the presence of at least one muon (single muon triggers) are used.

Since these triggers are designed for muons traveling close to the speed of light ($\beta \approx 1$), there is a loss of acceptance for CMLLP candidates with $\beta < 1$. The muon triggers impose a time window (trigger gate) on the muon scintillation counter hits. The trigger gate opens 15–30 ns before particles from a collision traveling at the speed of light reach a particular muon layer and closes 15–40 ns after that time. The effect of the trigger gate on events

with a pair of CMLLPs is more pronounced in di-muon triggers, where both slow moving particles must arrive within the trigger gate; see Fig. 2(a). The muon triggers are simulated by applying trigger efficiencies measured in $Z \to \mu\mu$ decays in data using a tag and probe method. Trigger efficiencies for CMLLPs are calculated using Monte Carlo (MC) simulations for different CMLLP masses. The overall selection efficiency, which is a product of the trigger gate efficiency and the efficiency for single muon triggers, for slow moving CMLLPs is higher for single muon triggers than that for dimuon triggers. We therefore use single muon triggers in the searches for a pair of CMLLPs as well as for a single CMLLP. The overall selection efficiency, including the efficiency of the trigger gate, for a single CMLLP is shown in Fig. 2(b).

A second time window (readout gate) is imposed on the muon signals during digitization. This gate opens 15–30 ns before particles from a collision traveling at the speed of light reach a particular muon layer and closes 70–90 ns after. In the search for a pair of CMLLPs both particles must be within the readout gate for the information to be recorded even though only one muon needs to be within the trigger gate for the trigger to be satisfied.

IV. MODELS AND SIGNAL GENERATION

Signal samples with direct production of a pair of CMLLPs are simulated using PYTHIA 6.409 [26]. Data events collected from random beam crossings are overlaid on simulated events to simulate additional interactions and detector noise. Production of CMLLPs through cascade decays from heavier new particles (such as squarks) is model dependent and has not been considered here. A GMSB model with a long-lived stau lepton NLSP, model line D in Ref. [27], is used to generate stau lepton pairs. The model parameters are given in Table I. The minimal supersymmetric standard model is used for generating long-lived gaugino-like charginos, higgsino-like charginos, and top squarks. The corresponding model parameters are given in Table II, where M_1, M_2, and M_3 are the mass parameters for U(1), SU(2), and SU(3) gauginos respectively, $\tan\beta$ is the ratio of the vacuum expectation values of the two Higgs doublets, and μ is the corresponding mass parameter. Long-lived top squarks are generated with PYTHIA and hadronized by linking with an algorithm external to PYTHIA. This algorithm [28] is applicable to any SUSY model that features a long-lived top squark. A set of 50,000 events is generated for each model and each mass point. A GEANT-based detector simulation models the detector response for the MC samples [29]. We have modified GEANT to treat our long-lived signal particles as heavy muons for purposes of tracking and estimating the $\mathrm{d}E/\mathrm{d}x$ of signal particles in the detector. Therefore, CMLLPs in MC samples have muon-like lifetimes. The detector geometry is described in detail in the simulation, which uses information on the position of the scintillation counters to evaluate the timing information of the hits in the counters. This information is used to calculate the TOF of the muons. Simulation of muon timing in the standard simulation software is corrected using information from data as described in Sec. V A. After the simulation of the detector response, a simulation of the electronics and digitization is performed. The simulated samples are then passed through the same reconstruction software that is used to reconstruct data.

Theoretical values of masses and couplings for different types of CMLLPs are calculated using SOFTSUSY [30]. This information is provided as input to PROSPINO [31] for the calculation of production cross sections and their uncertainties for different types and masses of CMLLPs.

V. ANALYSIS STRATEGY AND TECHNIQUES, AND SELECTION VARIABLES

With respect to their production at the primary vertex and penetration characteristics, CMLLPs are similar to prompt muons produced in $p\bar{p}$ collisions, but they travel at $\beta \approx 0.6$ to 0.8. The momenta of CMLLPs are distinctly higher than that of prompt muons despite their lower β, as shown in Fig. 3. In this figure we compare the highest and the second-highest p_T CMLLPs (simulated gaugino-like charginos of masses 100 GeV, 200 GeV, and 300 GeV) in an event with the highest and the second-highest p_T muons from $Z \to \mu\mu$ decays in data and MC events. Events are required to have two isolated muons with $p_T > 20$ GeV. The muons are required to be inconsistent with cosmic ray muons. All distributions are normalized to the same number of events. For $Z \to \mu\mu$ events, we require $70 < M_{\mu\mu} < 110$ GeV. The data and MC are compared in this mass range to determine the corrections to be applied to the MC. The CMLLPs considered here have a $\mathrm{d}E/\mathrm{d}x$ approximately proportional to $1/\beta^2$ which is much higher than the $\mathrm{d}E/\mathrm{d}x$ of an identified muon that is essentially a minimum ionizing particle [32]. Thus, TOF, which is used to calculate β, and $\mathrm{d}E/\mathrm{d}x$ of a particle can discriminate between CMLLP candidates and muons with $\beta \simeq 1$.

The Run IIa analysis, which searched for a pair of CMLLPs, used only the TOF of CMLLP candidates to distinguish them from prompt muons. The introduction of $\mathrm{d}E/\mathrm{d}x$ measurement into the Run IIb analyses allowed us to extend the search to events where only one CMLLP candidate could be detected. The Run IIa dataset was used to search for stau leptons, gaugino-like charginos, and higgsino-like charginos. The Run IIb analyses also searched for top squarks. Additional criteria needed for the selection of top squark candidates are described in detail in Sec. V C.

Results are presented in this article for stau leptons, gaugino-like charginos, and higgsino-like charginos from individual analyses as well as from a combination of Run IIa and Run IIb data with a total of 6.3 fb^{-1} integrated

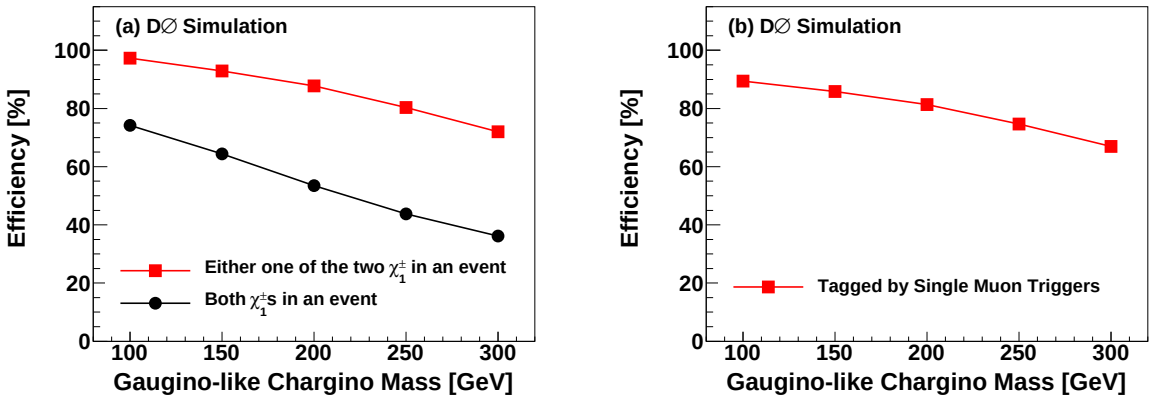

FIG. 2: (color online) Efficiency for slow-moving gaugino-like charginos of various masses to arrive within the L1 muon trigger gates. All events in this MC sample contain two gaugino-like charginos. (a) The black and red lines show the efficiencies for a pair of charginos, or a single chargino respectively, to be within the trigger gate. (b) Overall efficiency, which is a product of the trigger gate efficiency and the efficiency for single muon triggers, for the selection of single charginos.

Parameter	Description	Value
Λ_m	Scale of SUSY breaking	19 to 100 GeV
M_m	Messenger mass scale	2 Λ_m
N_5	Number of messenger fields	3
$\tan\beta$	Ratio of Higgs field vacuum expectation values	15
sign of μ	Sign of Higgsino mass parameter	+1

TABLE I: GMSB model parameters for stau lepton production.

Model	μ (GeV)	M_1 (GeV)	M_2 (GeV)	M_3 (GeV)	$\tan\beta$	Squark Mass (GeV)
Top squark	10,000	100	200	500	15	800
Gaugino-like chargino	10,000	$3M_2$	100 to 300	500	15	800
Higgsino-like chargino	100 to 300	100,000	100,000	500	15	800

TABLE II: Model parameters for top squark and chargino production.

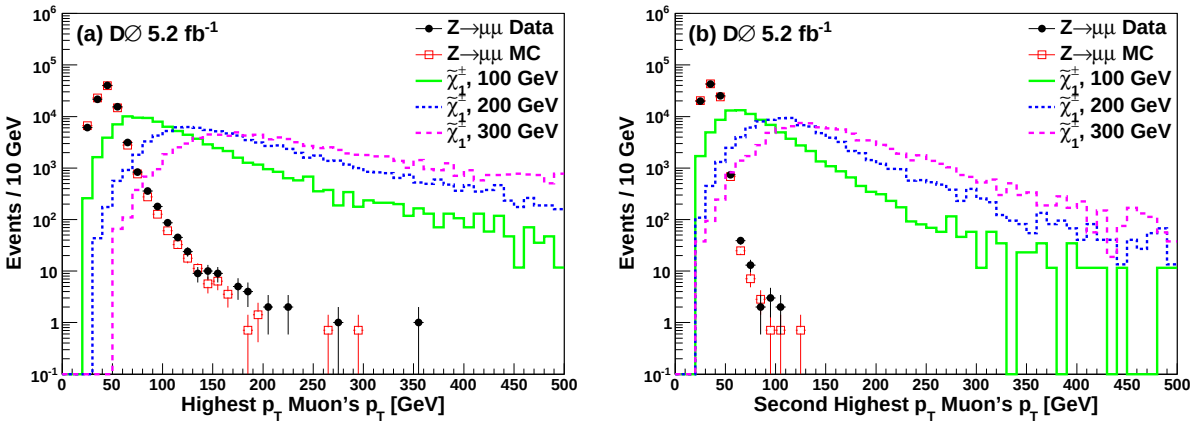

FIG. 3: (color online) Distributions of p_T of the (a) highest p_T and the (b) second-highest p_T muon in an event for $Z \to \mu\mu$ data and MC, and for simulated gaugino-like charginos with masses of 100 GeV, 200 GeV, and 300 GeV.

luminosity. To avoid double counting of events, the samples used for the two Run IIb analyses are constructed to be statistically independent. All events that pass the selection requirements used for the search for a pair of CMLLPs are removed from the data used for the single CMLLP search, resulting in an approximately 40% loss of signal acceptance for the single CMLLP search. The data and the background sample that are used in the search for single CMLLPs contain muons that originate mostly from the decays of W bosons. The number of such events changes by only about 2% due to this veto. Furthermore, we show results for searches for single top squarks and top squark pair production using 5.2 fb^{-1} integrated luminosity. A combination of the two analyses does not improve the result as explained in Sec. V C, and is not performed here.

A. Time-of-Flight Measurement

The TOF of a charged particle reaching the muon system can be calculated from the position of the scintillation counter that is hit and the corresponding time as has been described in Sec. II. A time offset is determined for each scintillation counter along with its associated cables and time digitizing electronics using a sample of muons from experimental data so that a time reading of zero is obtained for particles that originate at the center of the detector at the time of a beam-beam interaction and travel at the speed of light to the specific scintillation counter. These time offsets are imperfect and have fluctuated with, for example, the seasonal variation in the synchronization with the Tevatron accelerator clock ($\approx \pm 1$ ns) as shown in Fig. 4(a). The offsets are corrected by subtracting the relevant amount of deviation from each hit time in each scintillator. Figure 4(b) shows the mean of the time distribution of hits versus time after the offset correction. The time period for averaging is the duration for which p and $\bar{p}$ beams are circulated in the Tevatron accelerator after injection. This period is typically 12–24 hours.

It is observed that the MC simulation gives narrower time distributions than what is observed in data. Therefore, the TOF associated with a muon hit in MC is smeared to reflect the resolution of the time distribution of muons from Z boson decays in data. The amount of smearing depends on the location of the muon detector because of the differing sizes of the scintillation counters. Figures 5-7 show the time distributions in selected regions for layers A, B, and C in data and MC. There is some mismodeling at early times in the central C layer (Fig. 6(a)) and central bottom B layer (Fig. 7(c)) arising from the data-driven smearing that has been applied to the hit times of the muons in MC. This mismodeling is not in our signal region which is at large times and has a negligible effect on the results.

The value of β for a muon-like track is determined from a weighted average of the speeds β_i determined using times corresponding to individual scintillation counter hits on the track, the weights being the inverse of the squares of experimentally determined uncertainties. Figure 8 shows the $\langle\beta\rangle$ distribution of the highest and the second-highest p_T muons in data and in simulated gaugino-like chargino events.

We define the speed significance, which incorporates β with its uncertainty ($\sigma_{\langle\beta\rangle}$) as,

$$\text{speed significance} = \frac{1-\langle\beta\rangle}{\sigma_{\langle\beta\rangle}}. \tag{1}$$

Figure 9 shows speed significance distributions of the highest and the second-highest p_T muons in the event. Prompt muons will have speed significance near zero whereas CMLLPs will have positive speed significance. In the Run IIa analysis we use the product of the speed significances of the two muons, which will be positive for a pair of CMLLPs, as an additional criteria to separate signal events from background events. We also calculate the variable,

$$\text{speed } \chi^2/\text{dof} = \frac{1}{N-1}\sum\nolimits_i \frac{(\langle\beta\rangle-\beta_i)^2}{\sigma_i^2}, \tag{2}$$

where N is the number of scintillation counter hits associated with a muon track, β_i is the speed of the track corresponding to the hit in the ith scintillation counter and $\langle\beta\rangle$ is the weighted average of the speeds calculated for all scintillation counter hits on the track. For some tracks the measurement β_i from the hit on a particular layer is inconsistent with the β_j measurements from other layers causing a large contribution to the value of the speed χ^2/dof. To identify and remove this hit from the speed χ^2/dof calculation, hits on a muon track are removed one at a time and the speed χ^2/dof is recalculated with the rest of the hits. The set of hits with the lowest value of speed χ^2/dof is used to recalculate the speed provided it satisfies the qualities of a good muon candidate (described in Sec. II). Distributions of speed χ^2/dof for the highest p_T muon in data and in simulated gaugino-like chargino events are shown in Fig. 10(a).

The speed asymmetry, which is useful in the search for a CMLLP pair, can be defined for the two highest p_T muons in the event as:

$$\text{speed asymmetry} = \frac{|\beta_1-\beta_2|}{\beta_1+\beta_2}. \tag{3}$$

The speed asymmetry is near zero for both signal events and events containing two well measured muons, but will be large for events where one of the particles has a speed that has been mismeasured. Speed asymmetry distributions for data and for simulated gaugino-like chargino events are shown in Fig. 10 (b).

We have observed that the disagreements in $\langle\beta\rangle$ distributions from data and MC at small values of $\langle\beta\rangle$, visible in Fig. 8, can be removed by applying stringent requirements on either the speed χ^2/dof or the speed asymmetry

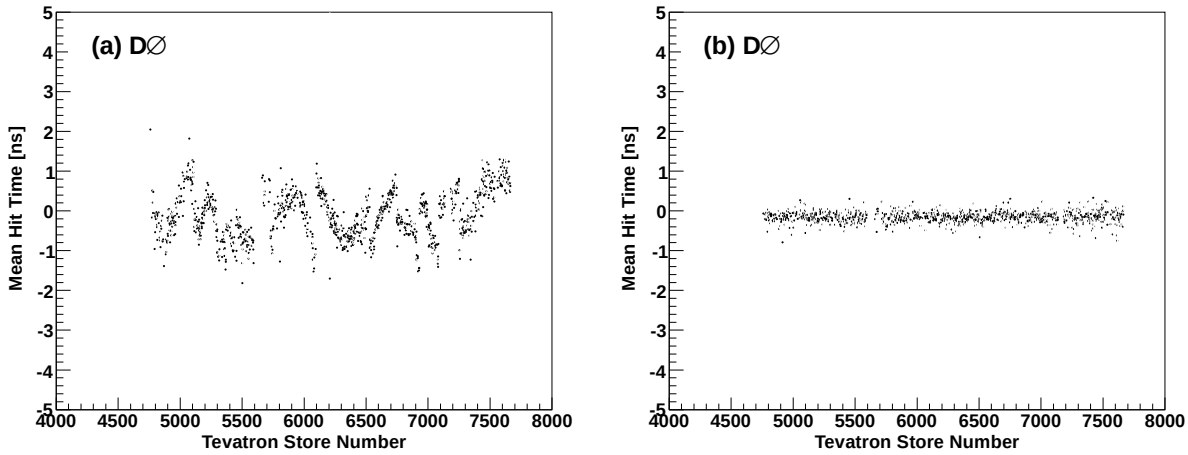

FIG. 4: (color online) Mean hit time as a function of the Tevatron store number in the forward region A-layer for muons from the decay of Z bosons in data (a) before correction and (b) after correction. A store is the time period for which p and $\bar{p}$ beams are circulated in the accelerator after injection. This period is typically 12–24 hours for the Tevatron. When the number of recorded times from $Z \to \mu\mu$ decays for a given store is large, a Gaussian function is fit to those times and the Gaussian mean is used. If the number of recorded times for a given store is small, the median of these times is used. These distributions cover the data taking period between June 2006 and March 2010.

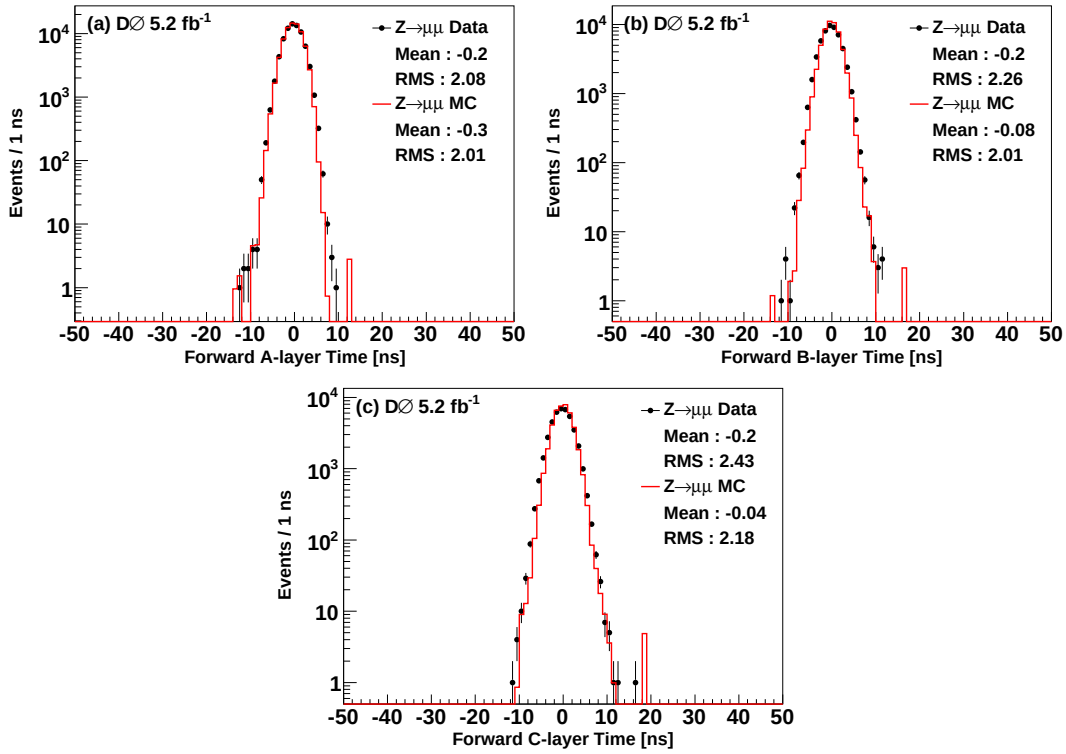

FIG. 5: (color online) Time distribution for scintillation counter layers A, B, and C in the forward muon system for times from $Z \to \mu\mu$ decays for data and MC events.

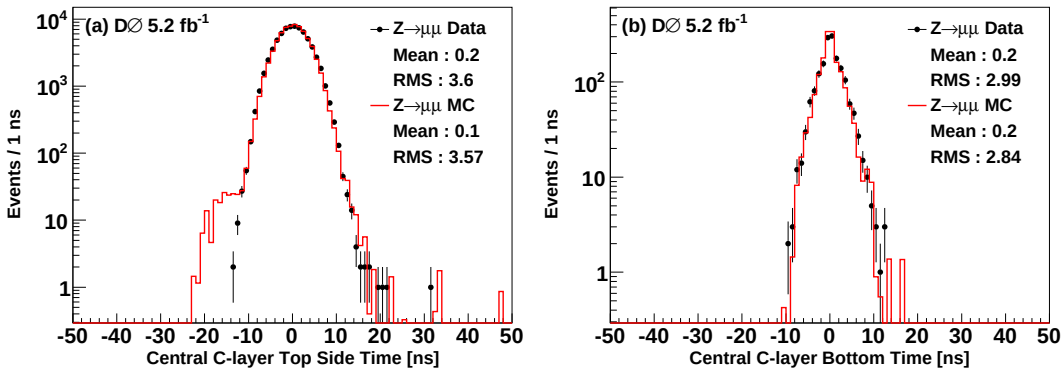

FIG. 6: (color online) Time distributions for scintillation counters in layer C, (a) top and sides, (b) bottom, in the central muon system for times from $Z \rightarrow \mu\mu$ decays for data and MC events.

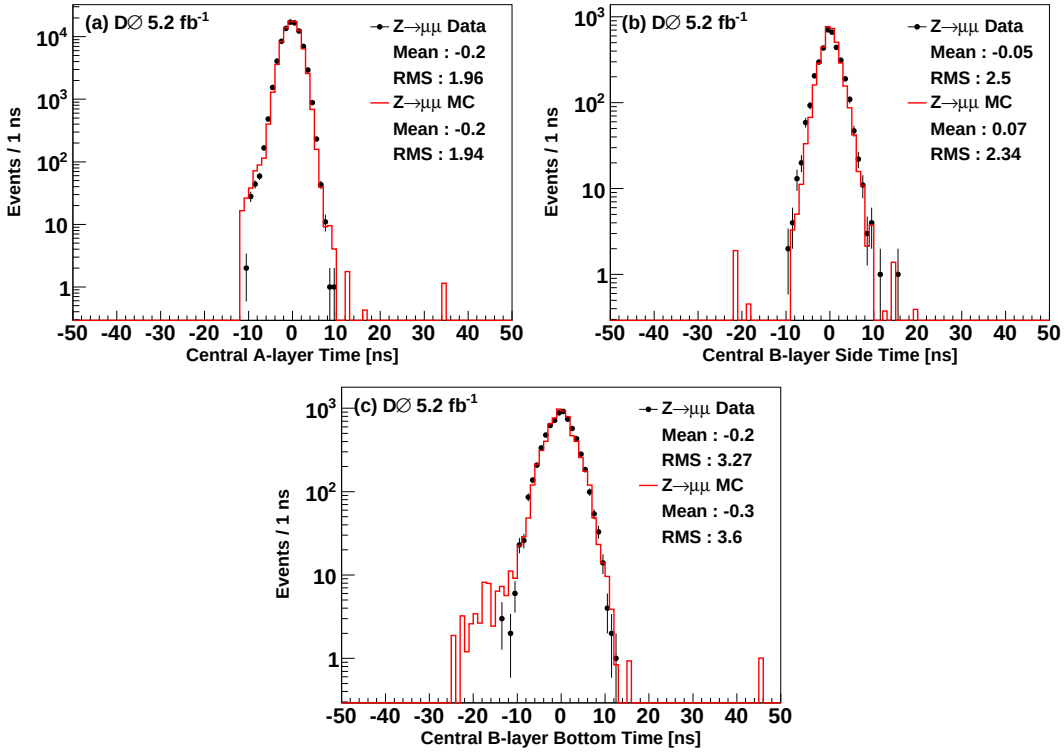

FIG. 7: (color online) Time distributions for scintillation counters in (a) layer A (top, bottom and sides), (b) layer B sides, and (c) layer B bottom, in the central muon system for times from $Z \rightarrow \mu\mu$ decays for data and MC events.

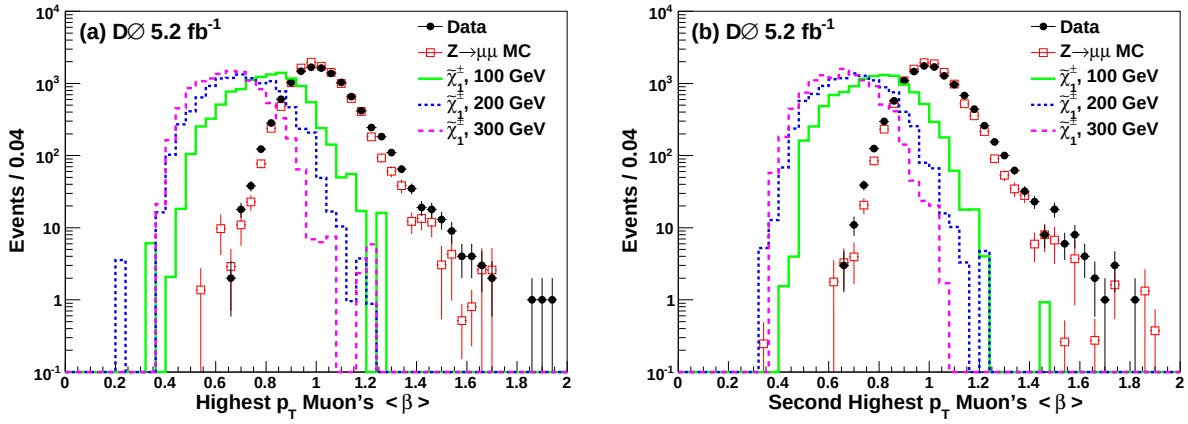

FIG. 8: (color online) Distributions of $\langle\beta\rangle$ of the (a) highest p_T and the (b) second-highest p_T muons. The distributions are normalized to the same number of events. Background is taken from $Z \to \mu\mu$ MC decays. The selection requirements are identical to those used in the pair CMLLP analysis, as described in Sec VI, except that the requirement $\langle\beta\rangle < 1$ is not imposed.

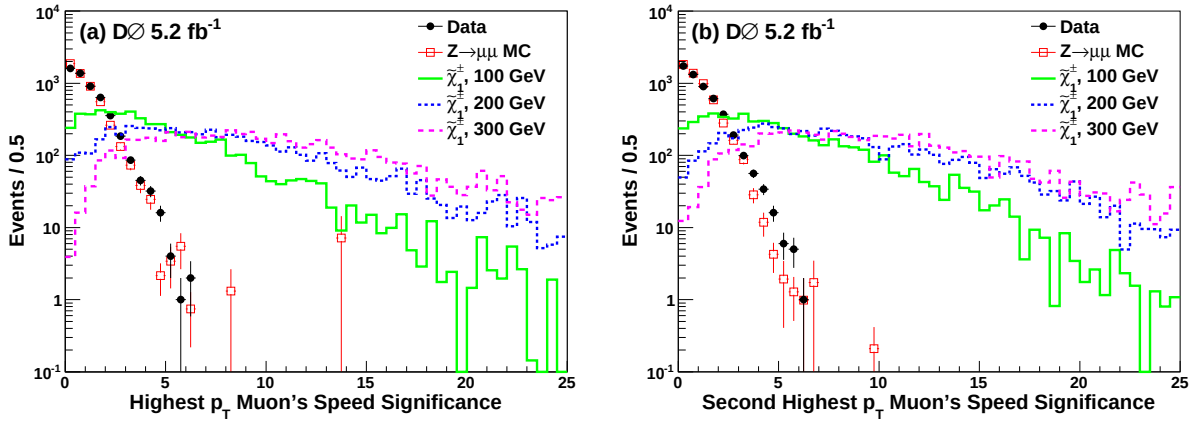

FIG. 9: (color online) Speed significance of the (a) highest p_T and the (b) second-highest p_T muons. The distributions are normalized to the same number of events. Background is taken from $Z \to \mu\mu$ MC. The selection requirements are identical to those used in the pair CMLLP analysis, as described in Sec VI, except that the requirement $\langle\beta\rangle < 1$ is not imposed.

distribution. The $\langle\beta\rangle$ distribution extends beyond 1 due to uncertainty in the measurement of velocity. There is some mismodeling for $\langle\beta\rangle > 1$, but this is not in our signal region. This disagreement is due to the background coming from mismeasured muons, which is characterized by large values of speed χ^2/dof or speed asymmetry, and not due to signal-like events, which are characterized by small values of speed χ^2/dof or speed asymmetry. We apply a requirement on the speed asymmetry of the two candidate CMLLPs in the search for a pair of CMLLPs as described in Sec. VI B. In the search for single CMLLPs we apply a requirement on the speed χ^2/dof of the candidate CMLLP as described in Sec VII B.

We correct the mismodeling in the speed χ^2/dof and the speed asymmetry distributions using a signal-free region (as described in Sec. VII B) in data. We compute the ratio of the speed χ^2/dof (or the speed asymmetry) distributions in data and $Z \to \mu\mu$ MC for events with 70 $< M_{\mu\mu} <$110 GeV, where the potential signal contribution is negligible. The value of this ratio is applied as a weight to all simulated events.

B. The dE/dx Measurement

The dE/dx of a particle is measured in the SMT. It is a calibrated average over SMT clusters and is corrected for the path length of the particle in the barrel or the disk sensor to reduce the dependence on the incident angle of the particle. The calculation of dE/dx excludes SMT clusters with the highest 20% of dE/dx values in order to minimize the contribution from Landau tails.

The average value of dE/dx is observed to decrease with increasing integrated luminosity [33] due to radiation damage to the silicon sensors. To correct for this

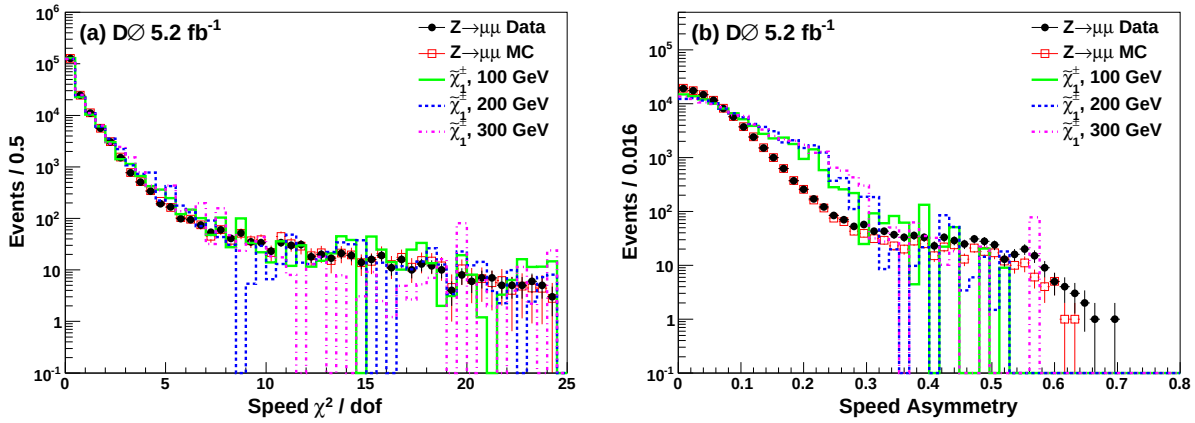

FIG. 10: (color online) (a) Distribution of speed χ^2/dof of the highest p_T muon in an event, and (b) speed asymmetry distribution of the highest and the second-highest p_T muons for $Z \to \mu\mu$ data, MC and signal (gaugino-like chargino with masses of 100 GeV, 200 GeV, and 300 GeV). The distributions are normalized to the same number of events. All events are required to have two isolated muons with p_T >20 GeV. For $Z \to \mu\mu$ events, we require $70 < M_{\mu\mu} < 110$ GeV. The muons are required to not be consistent with cosmic ray muons.

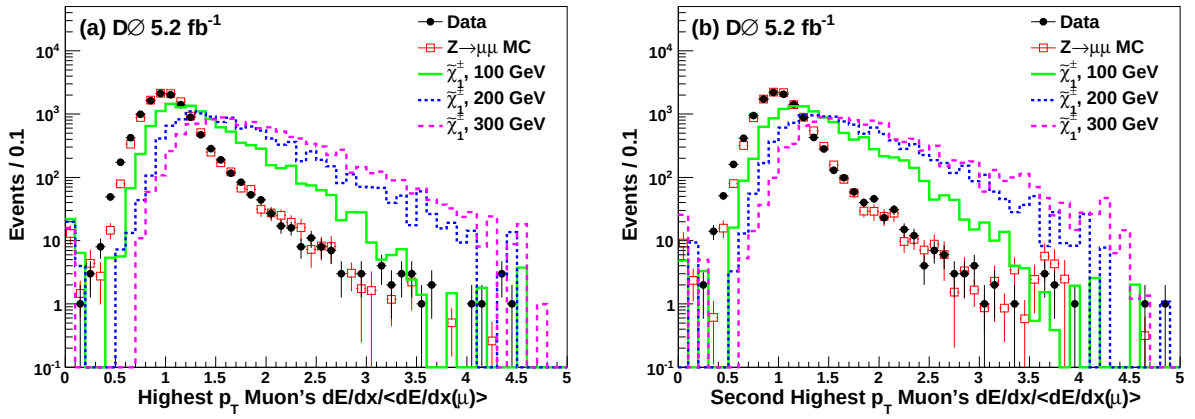

FIG. 11: (color online) Distributions of the adjusted dE/dx (described in Sec. V B) of the (a) highest p_T and the (b) second-highest p_T muons in data and the simulated chargino events. The distributions are normalized to the same number of events. The Background is taken from $Z \to \mu\mu$ MC. The selection requirements are identical to those used in the pair CMLLP analysis, as described in Sec VI.

effect, each dE/dx measurement is divided by the mean dE/dx.at dE/dx = 1, to facilitate the comparison between data and MC. The recalibrated dE/dx distribution is referred to as the "adjusted dE/dx". Figure 11 shows that the adjusted dE/dx distribution of muons from Z decays is well separated from that of candidate CMLLPs. Since the adjusted dE/dx distribution of muons from Z decays in data does not quite match the adjusted dE/dx of $Z \to \mu\mu$ MC events, a Gaussian smearing is applied to the adjusted dE/dx in MC to better describe the data. The precision of a particle's adjusted dE/dx depends on the number of SMT clusters used in its calculation. A new variable, dE/dx significance, is defined to estimate this dependence. If N_c is the number of SMT clusters on a track, and if the spread in the adjusted dE/dx distribution (which is a function of N_c) is $\sigma(dE/dx)_{N_c}$, then the dE/dx significance is:

$$\mathrm{d}E/\mathrm{d}x \text{ significance} = \frac{\mathrm{d}E/\mathrm{d}x - 1}{\sigma(\mathrm{d}E/\mathrm{d}x)_{N_c}}. \quad (4)$$

Figure 12 shows a distribution of the dE/dx significance for the highest p_T and the second-highest p_T muons in data and background, and for simulated gaugino-like charginos of 100–300 GeV masses. The two data points at high values of dE/dx significance have $\langle\beta\rangle$ close to 0.98 and are removed by the selection criteria described in Sec. VI B.

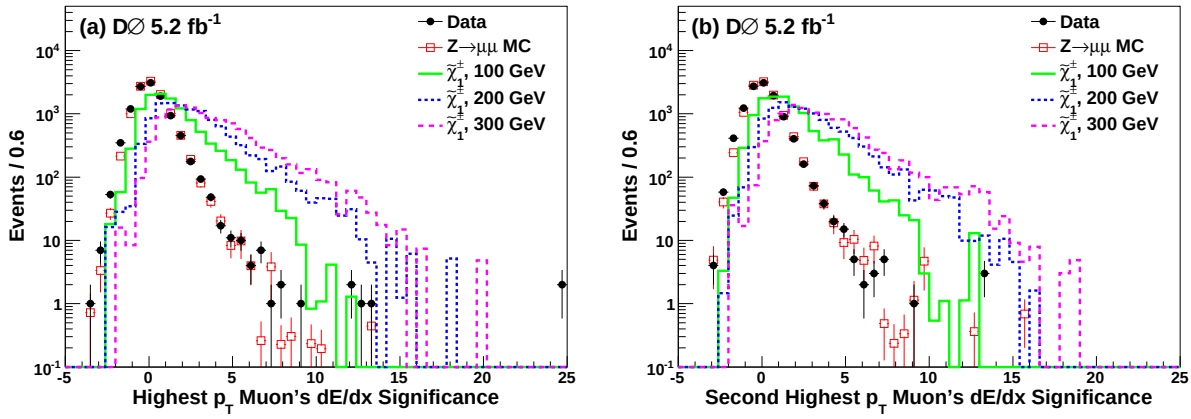

FIG. 12: (color online) Distributions of $\mathrm{d}E/\mathrm{d}x$ significance for the (a) highest p_T and the (b) second-highest p_T muons. The distributions are normalized to the same number of events. Background is taken from $Z \to \mu\mu$ MC. The selection requirements are identical to those used in the pair CMLLP analysis, as described in Sec VI.

C. Detection of Top Squarks

About 60% of top or anti-top squark hadrons will be charged after initial hadronization [34]. A top squark hadron passing through matter can exchange light quarks through nuclear interactions, changing the charge of the hadron. Because the detector has more quarks than antiquarks, after many nuclear interactions most of the top squark mesons become baryons, but anti-top squark antibaryons become anti-mesons. The charge of a top squark baryon can be 0, +1 or +2; the fractions are model dependent. We have assumed 2/3 of the stop baryons to be charged after undergoing many interactions in the detector material. Similarly, the charge of an anti-top squark anti-mesons can be 0 or −1. We assume anti-top squark anti-mesons to have a probability of 1/2 of being charged after passing through the detector material [35–37]. We also provide results assuming the top and anti-top squark hadrons do not flip charge at all for reference. In this case we only include a factor of 60% for the initial hadronization.

As can be seen in Fig. 1, the top squark or the anti-top squark hadron must be measured as charged at three locations while passing through the D0 detector to be reconstructed: after hadronization, after the calorimeter, and after the muon toroid. Both the calorimeter and the muon toroid contain enough material (10 and 6 interaction lengths respectively) to ensure that a top squark or anti-top squark hadron will undergo a large number of interactions when passing through them, randomizing its charge. Therefore, the probability of a top squark hadron to be charged at all three locations is 0.6 (at production) × 0.67 (at the end of the calorimeter) × 0.67 (at end of the muon toroid) = 0.27. Likewise, the probability of an anti-top squark hadron to be charged at all three locations is 0.6 × 0.5 × 0.5 = 0.15. The probability for a pair of top squark and anti-top squark hadrons both to be charged in all three locations is 0.27 × 0.15 = 0.04. The probability of at least one of the two being charged in all three locations is 0.27 × (1 − 0.15) + 0.15 × (1 − 0.27) + 0.27 × 0.15 = 0.38. We apply high enough p_T cuts on the reconstructed tracks so that the selected tracks have small curvatures and even the tracks with +2 charge are reconstructed and matched. For both the pair and the single CMLLP searches, these estimates of charge survival probabilities are applied as additional factors when the top squark MC is normalized to the expected number of events.

VI. SEARCH FOR EVENTS WITH A PAIR OF CMLLPS

With the selection variables described in Sec. V to provide discrimination of CMLLP signal over background, we describe below the selection criteria for the search for a pair of CMLLPs with 5.2 fb^{-1} of Run IIb integrated luminosity.

A. Background Sample

To model the background, one million events containing muons from decays of Z bosons were simulated using PYTHIA. Although a $Z \to \mu\mu$ MC sample is used to model the background, we do not assume that the background is only from $Z \to \mu\mu$ decays. Any source of muons that are not measured correctly contributes to the background. Since the p_T of the background muons have a wide range, we minimize the dependence of the analysis on the p_T of the selected tracks. Other than the initial requirement on the p_T of the tracks, the selection criteria do not depend any further on the p_T of the candidate CMLLPs. The important variables in this analysis,

β and normalized $\mathrm{d}E/\mathrm{d}x$, are largely independent of the p_T of the muon. The simulation has been tuned so that the β and the $\mathrm{d}E/\mathrm{d}x$ are well modeled as described in Sec. V A and B.

B. Event Selection

Events containing a pair of CMLLP candidates are selected by requiring that they contain at least one muon with $p_T > 20$ GeV and exactly two reconstructed, isolated muons of good quality with $|\eta| < 2$. The other selection criteria are:

- Number of SMT clusters, $(N_{SMT}) \geq 3$.
- $\langle\beta\rangle < 1$ for the two highest p_T muons.
- $\langle\beta\rangle$ asymmetry < 0.35.
- The highest p_T muon has $p_T > 55$ GeV and the second-highest p_T muon has $p_T > 50$ GeV.
- Matching χ^2 (between the track in the muon system and the central tracker) < 100.

Muons originating from cosmic rays are vetoed by checking the difference in their arrival times at the scintillation counter layers A and C shown in Fig. 13(a). The difference in the TOFs from the center of the detector to layer-A of two muons (Fig. 13(b)) also provides discrimination of muons produced in $p\bar{p}$ collisions from cosmic ray muons. The distance of closest approach (DCA) in the r-ϕ plane of each reconstructed muon track to the beam line, and the pseudo-acolinearity, $\Delta\alpha = |\Delta\phi + \Delta\theta - 2\pi|$, between the two muon tracks are also used to reject cosmic ray muons. These criteria are as follows:

- DCA in the r-ϕ plane of each muon < 0.2 cm.
- Difference between A-layer and C-layer times of a muon ≥ -10 ns.
- Absolute value of the difference in A-layer times between the two muons ≤ 10 ns.
- $\Delta\alpha \geq 0.05$.

These selection criteria are optimized to produce the best expected limits on the masses of CMLLP candidates.

The background sample is normalized to data events that pass the conditions described above and have invariant mass of the two highest p_T muons in each event within $70 < M_{\mu\mu} < 110$ GeV. The contribution of potential signal in this region is negligible. The number of data and background events selected using the above conditions are listed in Table III, and the efficiencies for signal events for various CMLLP candidates are given in Tables IV– VII.

A Boosted Decision Tree (BDT), as implemented in Ref. [38], is used to further discriminate signal events from background events. The BDT is trained using the expected signal and background distributions from MC, modified as described above. Half of the events are used to train the BDT while the remaining half are used to test the background model and signal response of the BDT. The variables used as inputs to the BDT are β, speed significance, normalized $\mathrm{d}E/\mathrm{d}x$, and $\mathrm{d}E/\mathrm{d}x$ significance for the highest p_T and the second-highest p_T muons. The distributions for these variables are shown in Figs. 8, 9, 11, and 12, where Figs. 8 and 9 show the distributions without the $\langle\beta\rangle < 1$ requirement. The correlation matrices for these variables for a stau signal with a mass of 300 GeV and muons from Z boson decays in MC are shown in Fig. 14(a) and (b), respectively. These figures show that there are non-trivial correlations between the variables and therefore MVA methods such as BDT, which will be able to take the correlations into account, are appropriate for this analysis. An example of the BDT output distribution is shown in Fig. 15 for simulated gaugino-like charginos of different masses. The BDT outputs for simulated stau leptons, top squarks, and higgsino-like chargino signals are shown in Figs. 24-26 in Appendix A. The final selection criteria on the BDT output are optimized to yield the best expected cross section limit in the no-signal hypothesis for each mass point, for each signal type.

C. Systematic Uncertainties

Systematic uncertainties are included in the estimation of cross section limits as follows. Each input parameter to the BDT distribution used to distinguish between signal and background is varied within its one standard deviation uncertainty and a new BDT distribution is produced for each variation for both signal and background models. The new BDT distributions are compared to the nominal ones and the average of the change in the occupancy of the BDT bins satisfying the selection requirement is taken as the systematic uncertainty due to that parameter. This procedure is applied to the sources of systematic uncertainties summarized below. These uncertainties are used in the limit calculation to model the effects of systematics in determining the limits.

- Uncertainty on the muon momentum scale in simulated samples is calculated by varying the p_T of the muon track by ± 1 standard deviation as measured in data.
- Time distributions for background and signal are modeled using $Z \to \mu\mu$ data events. We repeat the time smearing with time distributions of muons coming from $W \to \mu\nu$ decays in data and take the difference as the uncertainty.
- To account for effects of the calibration of individual scintillation counters on the L1 trigger gate, we shift the trigger gate by ± 1 ns and calculate the resulting change in signal efficiency.

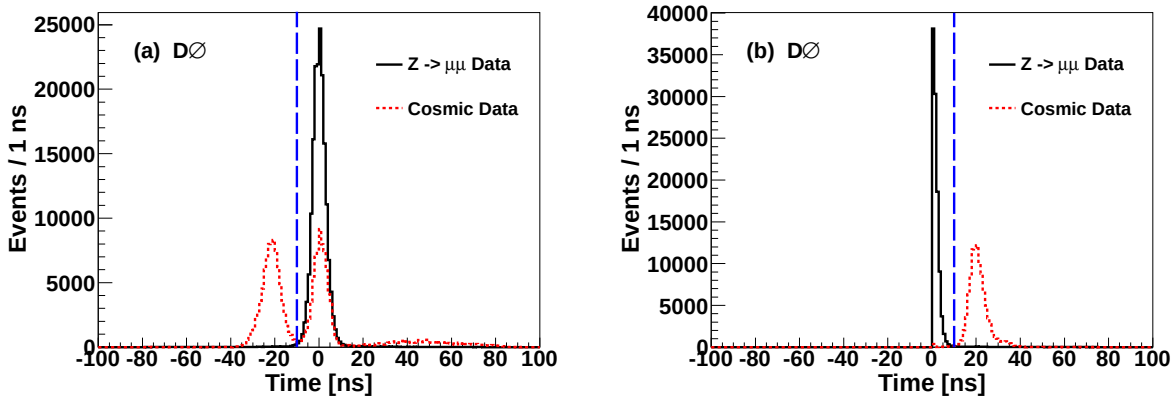

FIG. 13: (color online) (a) Difference between the A-layer and C-layer times for a single muon. There are two cosmic ray peaks for the two possible directions, away from or towards the $p\bar{p}$ collision vertex. (b) Absolute value of the difference between the A-layer times of the two muons in the event. The times shown in these plots are centered at zero for $\langle\beta\rangle = 1$ particles. This cosmic ray data was collected when there was no p or $\bar{p}$ beam in the Tevatron collider. Selection requirement on the time difference is shown with a blue vertical line.

Selection Criteria	Data events	Background Acceptance $Z \to \mu\mu$ MC (%)
Initial muon selection	231487	49.6
$N_\mu = 2$	178204	15.8
Trigger matching	125662	
Trigger probability		8.85
Cosmic veto	106941	7.57
L1 trigger gate (MC only), $N_{SMT} \geq 3$	98195	6.94
$\langle\beta\rangle < 1$, $\langle\beta\rangle$ asymmetry < 0.35	34376	2.17
$p_T^{\mu 1}$ >55, $p_T^{\mu 2}$ >50 GeV	709	0.03
Matching χ^2 <100	702	0.03

TABLE III: Selection efficiencies for data and background events before the application of BDT requirements for the search for a pair of CMLLPs with Run IIb data. Initially, events with at least one isolated muon of good quality and $p_T > 20$ GeV are required and a match between a muon and a central track is required based on χ^2.

M(stau lepton) in GeV Selection criteria	100	150	200	250	300
Initial muon selection	62.0	61.4	62.2	61.4	62.0
$N_\mu = 2$	25.0	25.2	25.6	25.6	25.5
Trigger probability	14.4	14.6	14.6	14.5	14.4
Cosmic veto	12.2	11.9	11.7	11.6	11.5
L1 trigger gate, $N_{SMT} \geq 3$	10.5	10.2	9.93	9.50	8.84
$\langle\beta\rangle$ <1, $\langle\beta\rangle$ asymmetry<0.35	9.08	9.44	9.45	9.17	8.62
$p_T^{\mu 1}$ >55, $p_T^{\mu 2} > 50$ GeV	8.35	9.30	9.42	9.15	8.60
Matching $\chi^2 < 100$	8.24	9.15	9.29	9.00	8.45

TABLE IV: Selection efficiencies (in %) before the application of BDT requirements for a pair of stau leptons in simulated events. The initial muon selection requires at least one isolated muon of good quality, matched to a central track with $p_T > 20$ GeV.

M(top squark) in GeV Selection criteria	100	150	200	250	300	350	400
Initial muon selection	50.6	54.9	57.9	59.6	58.6	58.3	57.7
$N_\mu = 2$	18.1	20.7	22.3	22.9	21.9	21.9	21.2
Trigger probability	10.4	12.0	12.9	13.2	12.5	12.5	12.0
Cosmic veto	8.67	9.81	10.5	10.5	9.72	9.71	9.31
L1 trigger gate, $N_{SMT} \geq 3$	7.79	8.79	9.26	8.83	7.63	6.76	5.34
$\langle\beta\rangle < 1$, $\langle\beta\rangle$ asymmetry < 0.35	7.16	8.28	8.93	8.63	7.45	6.65	5.24
$p_T^{\mu 1} > 55$, $p_T^{\mu 2} > 50$ GeV	5.97	8.06	8.85	8.61	7.44	6.64	5.24
Matching χ^2 <100	5.90	7.96	8.73	8.49	7.34	6.53	5.18
Charge survival efficiency (4%)	0.24	0.32	0.35	0.34	0.29	0.26	0.21

TABLE V: Selection efficiencies (in %) before the application of BDT requirements for a pair of top squarks in simulated events. The initial muon selection requires at least one isolated muon of good quality, matched to a central track with $p_T > 20$ GeV. The top squark charge survival efficiency is 4%.

M(gaugino-like chargino) in GeV Selection criteria	100	150	200	250	300
Initial muon selection	46.8	49.8	50.3	49.1	49.1
$N_\mu = 2$	16.2	17.9	18.3	17.6	17.7
Trigger probability	9.32	10.4	10.6	10.3	10.3
Cosmic veto	7.73	8.46	8.42	7.94	7.77
L1 trigger gate, $N_{SMT} \geq 3$	6.96	7.39	7.11	6.09	5.29
$\langle\beta\rangle$ <1, $\langle\beta\rangle$ asymmetry<0.35	6.36	6.98	6.88	5.95	5.16
$p_T^{\mu 1}$ >55, $p_T^{\mu 2}$ >50 GeV	5.23	6.67	6.77	5.92	5.14
Matching χ^2 <100	5.16	6.59	6.67	5.85	5.05

TABLE VI: Selection efficiencies (in %) before the application of BDT requirements for a pair of gaugino-like charginos in simulated events. The initial muon selection requires at least one isolated muon of good quality, matched to a central track with $p_T > 20$ GeV.

M(Higgsino-like chargino) in GeV Selection criteria	100	150	200	250	300
Initial muon selection	47.5	50.5	51.4	51.1	49.0
$N_\mu = 2$	17.1	18.6	19.3	19.0	18.0
Trigger probability	9.78	10.8	11.2	11.1	11.4
Cosmic veto	8.15	8.87	8.88	8.65	8.04
L1 trigger gate, $N_{SMT} \geq 3$	7.29	8.13	7.56	6.83	5.69
$\langle\beta\rangle < 1$, $\langle\beta\rangle$ asymmetry<0.35	6.57	7.70	7.31	6.68	5.59
$p_T^{\mu 1} > 55$, $p_T^{\mu 2} > 50$ GeV	5.40	7.39	7.23	6.65	5.56
Matching $\chi^2 < 100$	5.31	7.31	7.14	6.56	5.49

TABLE VII: Selection efficiencies (in %) before the application of BDT requirements for a pair of higgsino-like charginos in simulated events. The initial muon selection requires at least one isolated muon of good quality, matched to a central track with $p_T > 20$ GeV.

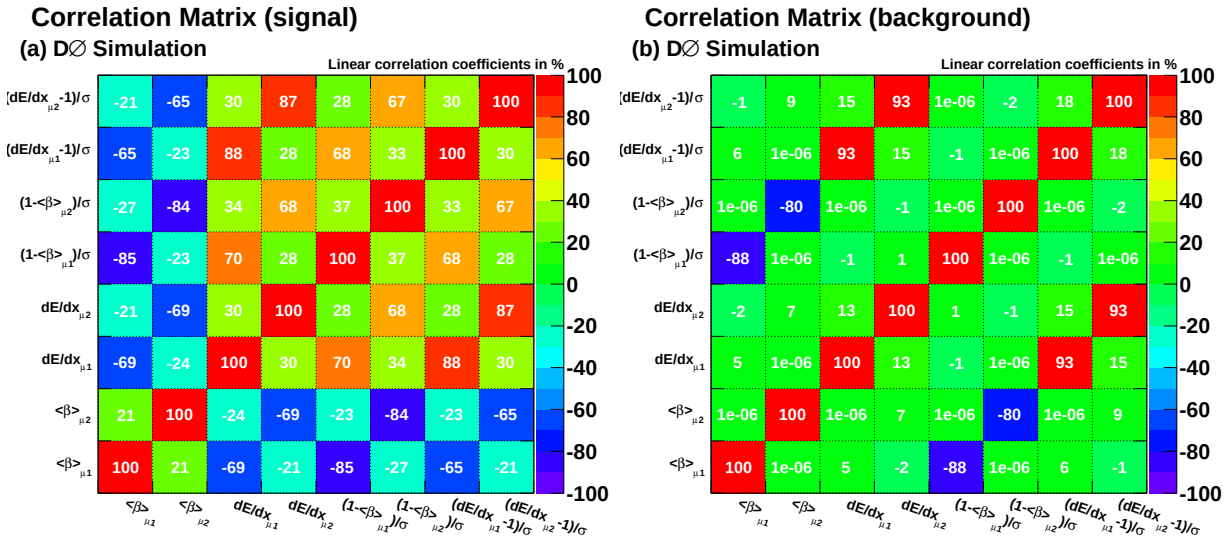

FIG. 14: (color online) Correlation matrix for different kinematic variables for (a) stau leptons of 300 GeV mass, and (b) background for the search of a pair of CMLLPs in the Run IIb data.

- Uncertainty due to the correction to the dE/dx measurement of selected tracks to equalize the degrading response due to radiation damage in silicon is evaluated by varying the correction factor by its ± 1 standard deviation uncertainty.

- dE/dx modeling uncertainty: the Gaussian smearing function applied to the dE/dx distribution of muons in MC is derived separately using $Z \to \mu\mu$ and $W \to \mu\nu$ data events. The difference between the BDT distributions obtained with the two methods is taken to be the systematic uncertainty due to dE/dx modeling.

- Theoretical values of production cross sections (described in Sec. IV) depend on the choice of parton distribution functions (PDF). Their effect is estimated by using the 40 CTEQ6.1M error PDFs [39] for signal and background. The variations from each of the error PDF sets and from the renormalization and factorization scale uncertainties are added in quadrature.

The remaining systematic uncertainties, given below, are added in quadrature to the uncertainties described above to obtain the total systematic uncertainties on signal acceptance and background prediction.

- The uncertainty in muon identification is a combination of the uncertainties due to selection of a muon (1.2%), central track reconstruction (1.4%), and isolation of the muon (0.9%).

- To determine the uncertainty in background normalization, the mass window for the control region is changed from $70 < M_{\mu\mu} < 110$ GeV to $60 < M_{\mu\mu} < 120$ GeV and $80 < M_{\mu\mu} < 100$ GeV.

- The MDTs have an asymmetric timing gate with a total length of 94 ns, which is not modeled in the MC. The signal from the earliest muon arrives at the MDTs within 74 ns of the beam crossing from $Z \to \mu\mu$ data. At most 1.2% of the CMLLPs that we consider will be in the forward muon system and will arrive at the MDTs more than 20 ns after a prompt muon. We have therefore introduced an additional 1.2% uncertainty on the signal acceptance.

- Uncertainty due to the speed asymmetry correction (described in Sec. V A) is estimated by the change in signal acceptance with and without the correction. This uncertainty is found to vary between 1% and 10% depending on the masses and types of CMLLPs. The value of this uncertainty is 3.6% for the background sample.

An uncertainty of 6.1% [33] on the integrated luminosity is applied to the signal efficiency. Systematic uncertainties for signal and background samples are listed in the second columns of Tables XVII and XVIII. The total systematic uncertainty for the background estimate is 18.2% and that for the signal acceptance is 11.2–15.2%, depending on the signal model and mass of the CMLLP.

D. Results

The signal acceptance, the background prediction, and the observed number of events after the BDT require-

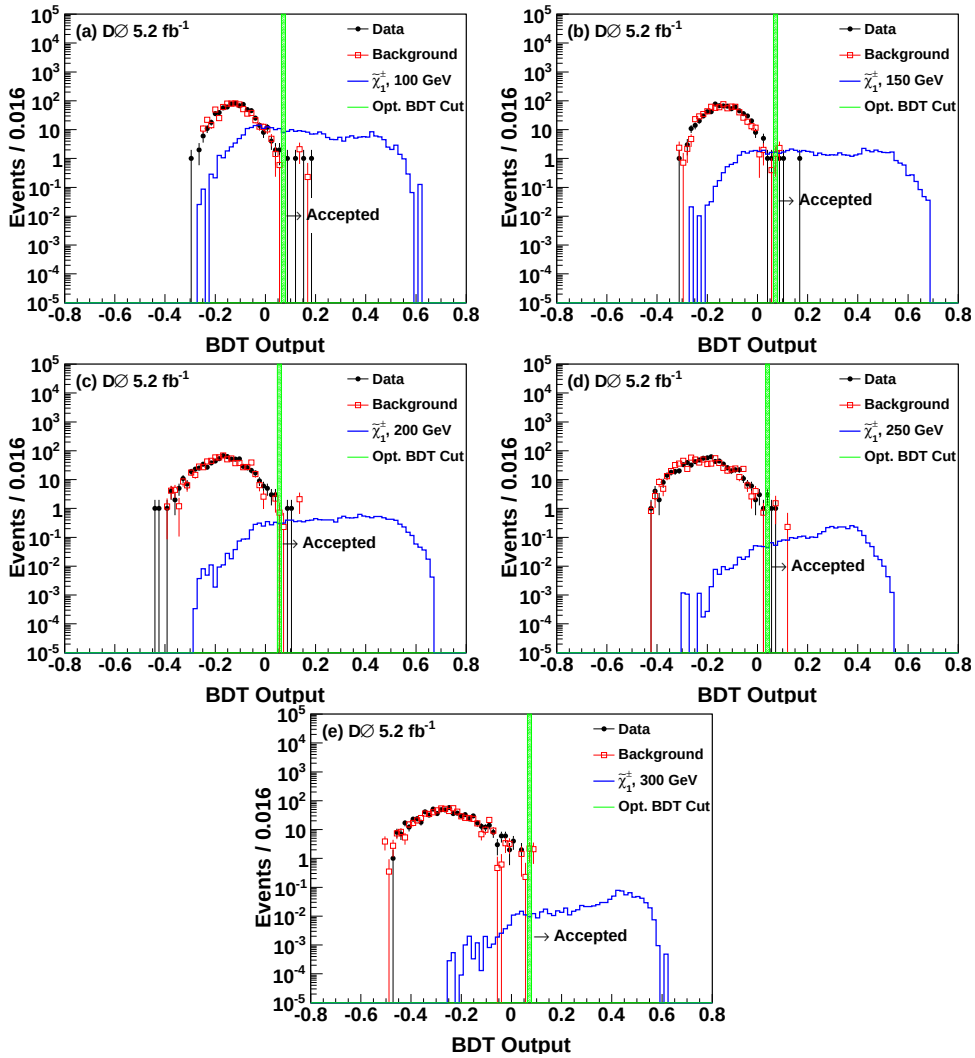

FIG. 15: (color online) BDT-output distributions for simulated gaugino-like chargino masses of 100–300 GeV in 50 GeV steps for the search for a CMLLP pair with the Run IIb data. Distributions are normalized to the expected number of events. Selection requirement on the BDT value is shown with a green vertical line. Note that a different BDT was constructed for each mass and the BDT selection requirement optimized separately for each mass.

ment are shown in Table VIII. These numbers are used as inputs to a modified Bayesian method [40] for calculating the limits on production cross sections at 95% C.L. Theoretical values of the production cross sections (described in Sec. IV) and observed and expected values of limits on the production cross sections of various CMLLPs are shown in Table IX and Fig. 16. The lower mass limits that are obtained from the cross section limits are 189 GeV for top squarks, 250 GeV for gaugino-like charginos, and 204 GeV for higgsino-like charginos. The limit on the mass of top squarks would increase to 280 GeV if we would include only the effects of their initial hadronization. If the intersection point of the -1 ($+1$) standard deviation band with the NLO cross section is used, then the mass limits shift down (up) by $\sim$1 GeV for charginos and by $\sim$20 GeV for top squarks.

VII. SEARCH FOR EVENTS WITH A SINGLE CMLLP

The following section describes the search for a single CMLLP in 5.2 fb^{-1} of integrated luminosity. More details can be found in Ref. [11].

A. Background Sample

The dominant background in the single CMLLP search is muons from the decays of W bosons, which is modeled with data. To define independent data and background samples, we select events using the transverse mass, M_T,

Mass (GeV)	Signal Acceptance (%)	Predicted Background	No. Observed Data events
Stau lepton			
100	3.27 ± 0.43	2.90 ± 1.77	3
150	5.24 ± 0.73	2.41 ± 1.58	4
200	7.24 ± 1.15	2.56 ± 1.63	3
250	6.90 ± 1.08	2.90 ± 1.77	4
300	7.25 ± 1.16	1.72 ± 1.25	0
Top squark			
100	0.12 ± 0.01	2.41 ± 1.58	2
150	0.12 ± 0.01	2.41 ± 1.58	3
200	0.24 ± 0.04	2.71 ± 1.63	3
250	0.26 ± 0.04	2.41 ± 1.58	2
300	0.25 ± 0.04	2.41 ± 1.58	1
350	0.25 ± 0.04	2.41 ± 1.58	3
400	0.20 ± 0.04	1.72 ± 1.25	1
Gaugino-like chargino			
100	3.67 ± 0.51	2.41 ± 1.58	4
150	4.76 ± 0.59	2.41 ± 1.58	3
200	5.57 ± 0.91	2.41 ± 1.58	2
250	5.20 ± 0.82	1.72 ± 1.25	1
300	4.63 ± 0.72	2.17 ± 1.37	0
Higgsino-like chargino			
100	2.79 ± 0.31	2.41 ± 1.58	1
150	4.36 ± 0.45	2.41 ± 1.58	0
200	5.74 ± 0.66	1.72 ± 1.25	2
250	5.62 ± 0.71	1.72 ± 1.25	1
300	5.29 ± 0.64	2.17 ± 1.37	3

TABLE VIII: Signal acceptance, number of predicted background events, and number of observed events in the search for a pair of CMLLPs with Run IIb data after each BDT selection. The error is a sum in quadrature of statistical and systematic errors.

of the W boson given by

$$M_T = \sqrt{(p_T{}^{\mu} + \not{E}_T)^2 - (p_x + \not{E}_x)^2 - (p_y + \not{E}_y)^2}. \quad (5)$$

Here $p_T{}^{\mu}$ is the transverse momentum of the muon and $\not{E}_T$ is the total unbalanced momentum transverse to the beamline as measured in the calorimeter and corrected for the muons. Events with $M_T \leq 200$ GeV and $\langle\beta\rangle < 1$ are selected for the background sample and events with $M_T > 200$ GeV and $\langle\beta\rangle < 1$ constitute the search sample. Figure 17 shows a distribution of M_T for single muon events from data and for higgsino-like chargino MC events.

B. Event Selection

The criteria to select events with one or more CMLLPs are similar to those used in the search for a pair of CMLLPs (Sec. VI B). Events satisfying a suite of single muon triggers are required to contain an isolated muon of good quality (described in Sec. VI B) within $|\eta| < 1.6$. The muon must originate at the $p\bar{p}$ interaction vertex and must satisfy the following criteria:

- $p_T > 60$ GeV.
- speed $\chi^2/\text{dof} < 2$.

If there is more than one such muon in the event, only the highest p_T muon is considered as the CMLLP candidate. To ensure that selected muons do not originate from cosmic rays, we require the DCA in the r-ϕ plane of the selected muon track to the beam line to be less than 0.2 cm and the difference between A-layer and C-layer times to be ≥ -10 ns.

If there is a second muon passing all the selection criteria, conditions to remove the cosmic ray events are the same as in the search for CMLLP pairs (described in Sec. VI B). The selection criteria and the corresponding efficiencies for number of events in data and the CMLLP signals are given in Tables X – XIV.

Since the background is modeled using data, it is necessary to normalize it to data in a signal-free region.

Mass (GeV)	NLO cross section (pb)	$\sigma_{95}^{\rm obs}$ (pb)	$\sigma_{95}^{\rm exp}$ (pb)
Stau lepton			
100	$0.0120^{+0.0006}_{-0.0008}$	0.038	$0.031^{+0.020}_{-0.002}$
150	$0.0021^{+0.0001}_{-0.0002}$	0.029	$0.020^{+0.011}_{-0.010}$
200	$0.00050^{+0.00003}_{-0.00002}$	0.018	$0.015^{+0.009}_{-0.003}$
250	$0.00010^{+0.00001}_{-0.00001}$	0.020	$0.016^{+0.004}_{-0.004}$
300	$0.000030^{+0.000003}_{-0.000004}$	0.009	$0.012^{+0.008}_{-0.002}$
Top squark			
100	$15.60^{+5.40}_{-4.00}$	0.89	$0.89^{+0.45}_{-0.23}$
150	$1.58^{+0.53}_{-0.42}$	1.05	$0.86^{+0.24}_{-0.29}$
200	$0.270^{+0.088}_{-0.068}$	0.42	$0.42^{+0.11}_{-0.09}$
250	$0.056^{+0.020}_{-0.014}$	0.40	$0.40^{+0.11}_{-0.09}$
300	$0.0130^{+0.0048}_{-0.0039}$	0.32	$0.40^{+0.14}_{-0.09}$
350	$0.0032^{+0.0012}_{-0.0009}$	0.52	$0.42^{+0.09}_{-0.08}$
400	$0.00075^{+0.0003}_{-0.0002}$	0.40	$0.40^{+0.05}_{-0.06}$
Gaugino-like chargino			
100	$1.33^{+0.08}_{-0.07}$	0.041	$0.028^{+0.010}_{-0.002}$
150	$0.240^{+0.014}_{-0.010}$	0.022	$0.025^{+0.005}_{-0.005}$
200	$0.0570^{+0.0034}_{-0.0030}$	0.019	$0.019^{+0.005}_{-0.003}$
250	$0.0150^{+0.0011}_{-0.0010}$	0.162	$0.016^{+0.002}_{-0.002}$
300	$0.0042^{+0.0004}_{-0.0003}$	0.013	$0.023^{+0.003}_{-0.007}$
Higgsino-like chargino			
100	$0.380^{+0.023}_{-0.017}$	0.029	$0.037^{+0.007}_{-0.005}$
150	$0.0740^{+0.0040}_{-0.0038}$	0.019	$0.024^{+0.003}_{-0.003}$
200	$0.0190^{+0.0012}_{-0.0010}$	0.018	$0.018^{+0.004}_{-0.003}$
250	$0.0053^{+0.0004}_{-0.0004}$	0.015	$0.015^{+0.002}_{-0.005}$
300	$0.0015^{+0.0001}_{-0.0001}$	0.024	$0.020^{+0.006}_{-0.003}$

TABLE IX: NLO cross section and 95% C.L. limits (σ_{95}) for the search for a pair of CMLLPs in the Run IIb data. The top squark charge survival efficiency is 4% (see text).

Selection Criteria	Number of Events	
Initial Muon Selection	345173	
Isolated muon	141008	
Trigger matching	79983	
Cosmic veto	79096	
$N_{SMT} \geq 3$	57532	
$p_T > 60$ GeV	56466	
$\langle\beta\rangle < 1$, Speed $\chi^2/dof < 2$	27876	
Matching $\chi^2 \leq 100$	27742	
	Background ($M_T \leq 200$ GeV)	Data ($M_T > 200$ GeV)
	22368	5374

TABLE X: Selection efficiencies for data in the search for single CMLLPs before applying the BDT selection requirements. Initially, events with at least one isolated muon of good quality and $p_T > 20$ GeV are required and a match between a muon and a central track is required based on χ^2.

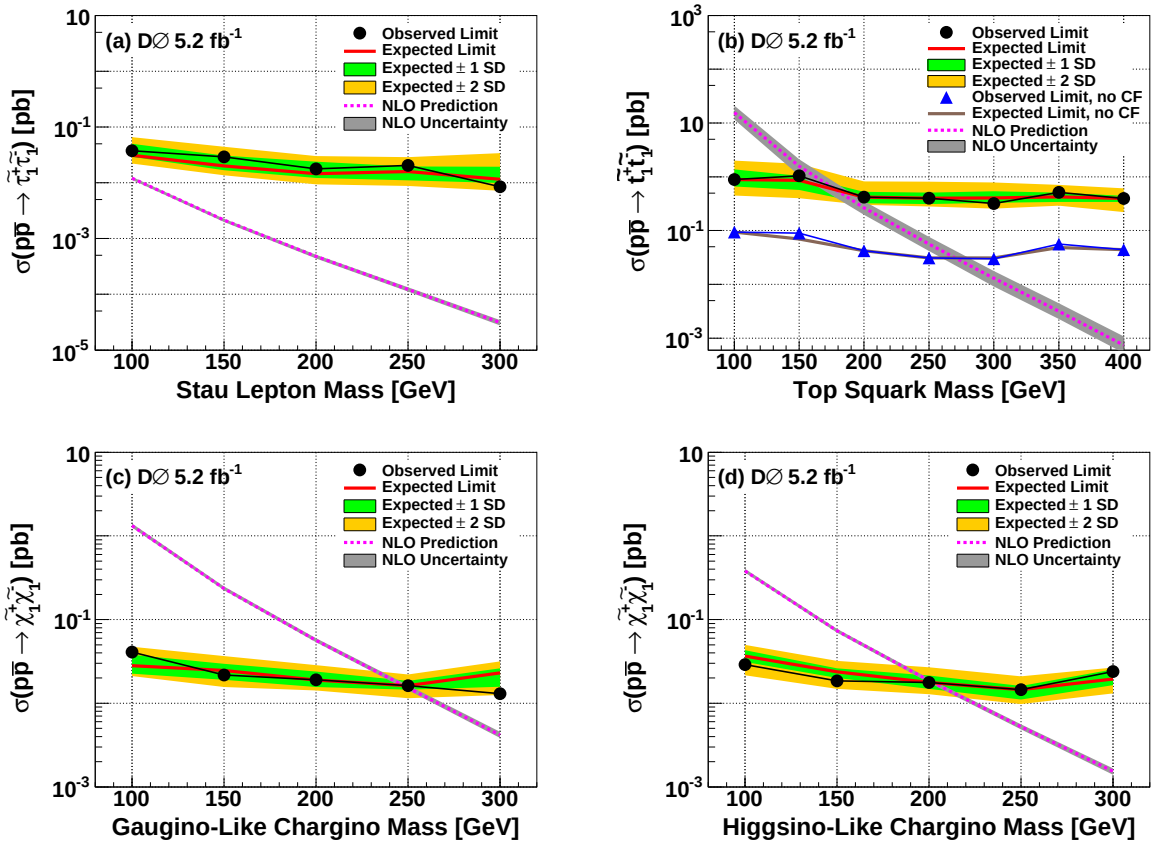

FIG. 16: (color online) 95% C.L. limits on production cross sections of a pair of stau leptons, top squarks, gaugino-like charginos, and higgsino-like charginos as a function of their masses from the search for a pair of CMLLPs with Run IIb data. "CF" is the scenario without charge flipping. ±1 SD and ±2 SD are the 1 and 2 standard deviation bands respectively around the expected limit curves.

M(stau lepton) in GeV Selection criteria	100	150	200	250	300
Initial muon selection	68.9	67.9	68.9	68.1	68.5
Isolated muon	59.1	59.5	60.6	60.2	60.8
Trigger probability	31.5	31.2	31.4	31.0	31.0
Cosmic veto	27.9	26.2	25.3	27.3	26.1
L1 trigger gate, $N_{SMT} \geq 3$	22.2	19.6	18.0	18.0	15.6
$p_T > 60$ GeV	20.3	19.4	18.0	18.0	15.6
$\langle\beta\rangle < 1$, Speed χ^2/dof < 2	16.9	16.5	15.6	15.7	13.7
Matching $\chi^2 \leq 100$	16.8	16.4	15.5	15.6	13.6
$M_T > 200$ GeV	14.4	15.6	15.2	15.4	13.6

TABLE XI: Selection efficiencies (in %) for a single stau lepton in MC events. Initially, events with at least one isolated muon of good quality and $p_T > 20$ GeV are required and a match between a muon and a central track is required based on χ^2.

M(top squark) in GeV Selection criteria	100	150	200	250	300	350	400
Initial muon selection	56.9	62.3	65.6	56.6	67.2	66.9	66.5
Isolated muon	46.0	52.0	55.8	47.0	57.3	57.3	56.6
Trigger probability	24.9	27.6	29.3	25.3	29.4	29.3	28.8
Cosmic veto	21.1	23.3	26.2	24.3	24.6	23.3	24.6
L1 trigger gate, $N_{SMT} \geq 3$	15.7	16.8	18.0	15.3	14.3	11.8	10.6
$p_T > 60$ GeV	13.0	16.3	18.0	15.3	14.2	11.8	10.6
$\langle\beta\rangle < 1$, Speed $\chi^2/dof < 2$	11.1	14.3	15.7	13.5	12.5	10.4	9.3
Matching $\chi^2 \leq 100$	11.0	14.1	15.6	13.4	12.4	10.4	9.3
$M_T > 200$ GeV	8.6	13.2	15.2	13.3	12.4	10.3	9.3
Charge survival efficiency (38%)	3.3	5.0	5.8	5.0	4.7	3.9	3.5

TABLE XII: Selection efficiencies (in %) for a single top squark in MC events. Initially, events with at least one isolated muon of good quality and $p_T > 20$ GeV are required and a match between a muon and a central track is required based on χ^2.

M(gaugino-like chargino) in GeV Selection criteria	100	150	200	250	300
Initial muon selection	51.7	54.7	55.4	54.3	53.8
Isolated muon	41.3	44.6	45.7	44.7	44.9
Trigger probability	22.7	24.3	24.7	24.2	24.1
Cosmic veto	21.0	20.8	21.0	19.9	19.7
L1 trigger gate, $N_{SMT} \geq 3$	15.5	13.8	12.4	10.0	8.4
$p_T > 60$ GeV	12.2	13.1	12.3	10.0	8.4
$\langle\beta\rangle < 1$, Speed $\chi^2/dof < 2$	10.4	11.7	11.0	8.9	7.4
Matching $\chi^2 \leq 100$	10.3	11.6	10.9	8.9	7.4
$M_T > 200$ GeV	7.8	10.6	10.6	8.8	7.4

TABLE XIII: Selection efficiencies (in %) for a single gaugino-like chargino in simulated events. Initially, events with at least one isolated muon of good quality and $p_T > 20$ GeV are required and a match between a muon and a central track is required based on χ^2.

M(higgsino-like chargino) in GeV Selection criteria	100	150	200	250	300
Initial muon selection	52.4	55.6	56.6	56.1	53.9
Isolated muon	42.2	45.8	47.0	47.0	45.3
Trigger probability	23.1	25.0	25.3	25.3	24.2
Cosmic veto	21.1	23.4	23.7	21.3	20.1
L1 trigger gate, $N_{SMT} \geq 3$	15.9	15.9	14.5	11.4	9.1
$p_T > 60$ GeV	12.7	15.2	14.4	11.3	9.1
$\langle\beta\rangle < 1$, Speed $\chi^2/dof < 2$	10.8	13.4	12.7	10.1	8.2
Matching $\chi^2 \leq$100	10.8	13.4	12.7	10.1	8.1
$M_T > 200$ GeV	8.3	12.2	12.4	10.0	8.1

TABLE XIV: Selection efficiencies (in %) for a single higgsino-like chargino in MC events. Initially, events with at least one isolated muon of good quality and $p_T > 20$ GeV are required and a match between a muon and a central track is required based on χ^2.

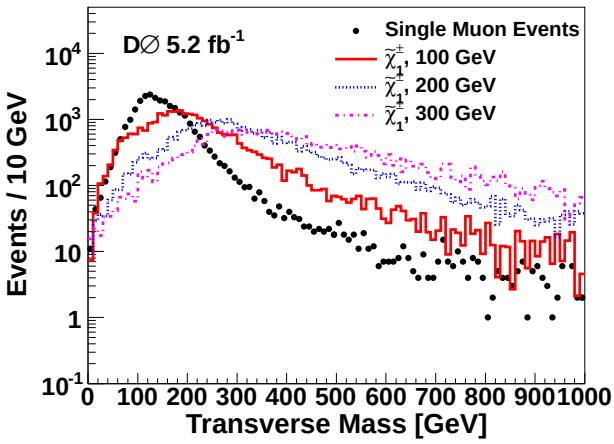

FIG. 17: (color online) The transverse mass M_T for single muon events and higgsino-like chargino events with chargino masses 100 GeV, 200 GeV, and 300 GeV. The single muon event sample satisfies all of the selection criteria described in Table X except the M_T cut, which separates the data and background samples. All the selection criteria described in Table XIV have been applied to the charginos except the $M_T > 200$ GeV cut. The distributions have been normalized to the same number of events.

Events containing muons with measured $\langle\beta\rangle \geq 1$ are used to define a signal-free region. Signal-free control events contain muons with $\langle\beta\rangle \geq 1$ and $M_T \leq 200$ GeV, and signal-free data contain muons with $\langle\beta\rangle > 1$ and $M_T > 200$ GeV. If the number of background events is N_B, the number of signal-free control events is N_{SFC}, and the number of signal-free data events is N_{SFD}, then the number of normalized background events, N_{NB}, can be expressed as

$$N_{NB} = N_B \frac{N_{SFD}}{N_{SFC}}. \tag{6}$$

The key variables used for discrimination between signal and background are $\langle\beta\rangle$ and $\mathrm{d}E/\mathrm{d}x$. These variables are anti-correlated for candidate tracks originating from signal, but not for those originating from background. Figure 18 shows the adjusted $\mathrm{d}E/\mathrm{d}x$ as a function of $\langle\beta\rangle$ for simulated gaugino-like charginos, background, and data. The variables $\langle\beta\rangle$, speed significance, number of scintillation counter hits, $\mathrm{d}E/\mathrm{d}x$, $\mathrm{d}E/\mathrm{d}x$ significance, and N_{SMT} are used as inputs to a BDT. The BDT is trained to distinguish between signal and background events using signal events from MC and background events from data. Half the input events are used for training, while the other half are used as a test sample to model the background and signal response of the BDT. The distributions of the BDT input variables are shown in Figs. 19 and 20.

An example of the BDT-output distribution is shown in Fig. 21 for simulated gaugino-like charginos for masses 100–300 GeV. The BDT-output distributions for simulated stau lepton, top squark, and higgsino-like charginos, after being normalized to the expected number of events, are shown in Figs. 27-29 in Appendix A. These BDT distributions are used as input to a modified frequentist limit calculation employing a log-likelihood ratio (LLR) test statistic [41, 42] to obtain 95% C.L. cross section limits. To minimize the degrading effects of systematic uncertainties on the search sensitivity, the signal and background are fitted to the observed data by maximizing a likelihood function over the systematic uncertainties for both the background-only and the signal-plus-background hypotheses.

C. Systematic Uncertainties

The sources of systematic uncertainties and their estimation are similar to the search for CMLLP pairs, described in Sec. VI C. A parameter is varied within its uncertainty and the change is propagated through the entire analysis to produce a BDT distribution. The systematic uncertainties can be divided into two categories, "normalization" and "shape" uncertainties. Normalization uncertainties affect only the overall event rate whereas the shape uncertainties can also change the differential distribution.

The systematic uncertainty due to uncertainty in luminosity (6.1%) and in muon reconstruction efficiency (2.1%) are normalization uncertainties. The other sources of normalization uncertainties are: the background normalization uncertainty due to the choice of the cuts on $\langle\beta\rangle$ (7.2%) and M_T (2.2%), the muon p_T resolution uncertainty (0.2%), the $\mathrm{d}E/\mathrm{d}x$ correction uncertainty ($< 0.1\%$), the $\mathrm{d}E/\mathrm{d}x$ smearing uncertainty (0.2%), and the speed χ^2/dof correction uncertainty (0.4%). The systematic uncertainty for the speed χ^2/dof correction is determined by repeating the data to MC correction (described in Sec. V A) with a MC sample of $W \to \mu\nu$ decays and then taking the difference between the two corrections as the uncertainty. The uncertainties due to the choice of PDF, and the $\mathrm{d}E/\mathrm{d}x$ correction are the same as in Sec. VI C. The systematic uncertainties due to the width of the L1 timing gate, and the timing simulation change with the output value of the BDT and therefore are shape systematics. The average uncertainty for the L1 timing gate width is 4% and that for the timing simulation is 7%. These uncertainties are summarized in the third columns of Tables XVII, and XVIII.

D. Results

For the single CMLLP search with 5.2 fb^{-1} integrated luminosity, 95% C.L. upper limits on production cross sections for stau leptons, top squarks, gaugino-like, and higgsino-like charginos are shown in Table XV and in Fig. 22. Limits are set on production cross section of

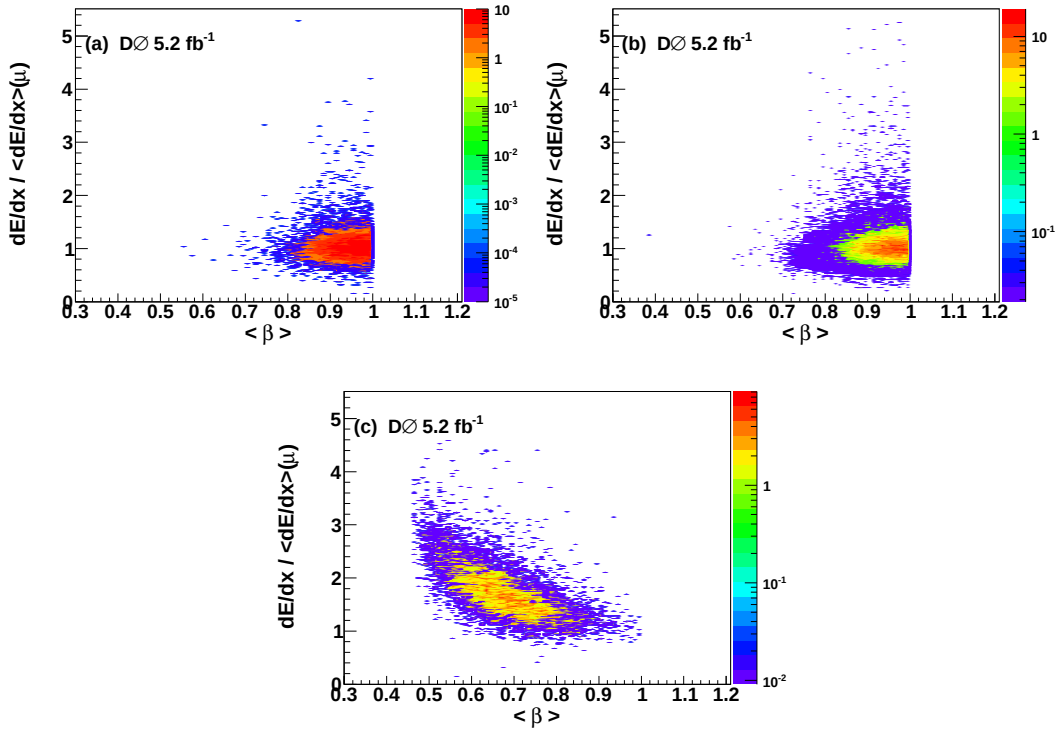

FIG. 18: (color online) Adjusted $\mathrm{d}E/\mathrm{d}x$ versus $\langle\beta\rangle$ for (a) data events, (b) background (data events with $M_T \leq 200$ GeV), (c) MC sample for gaugino-like charginos with mass of 300 GeV.

stau leptons from 0.05 pb to 0.006 pb, for stau lepton masses in the range between 100 GeV and 300 GeV. Pair-produced long-lived top squarks are excluded below masses of 285 GeV. If we only include the effects of initial hadronization of top squarks and do not include the effects of charge flipping during their passage through the detector, the lower limit on long-lived top squark mass is found to be 305 GeV. Pair-produced long-lived gaugino-like charginos are excluded below masses of 267 GeV, and higgsino-like charginos below masses of 217 GeV. They are identical to those presented in [11]. Using the intersection of the -1 ($+1$) standard deviation band with the NLO cross section, the mass limits shift down (up) by 1 GeV for charginos and by 10 GeV for top squarks.

VIII. RUN IIa RESULT

The search for a pair of CMLLPs in 1.1 fb^{-1} of Run IIa integrated luminosity utilizes the TOF measurement in addition to other kinematic variables to select events with candidate CMLLPs [5]. The CMLLP candidates in this analysis are staus, gaugino-like, and higgsino-like charginos. The principal background comes from mismeasured muons from the decays of the Z boson. Table XVI presents the signal acceptance, the number of predicted background events, and the number of observed events in this analysis. In the absence of any signal, limits of 206 GeV and 171 GeV are set on masses of gaugino-like charginos and higgsino-like charginos, respectively. Limits on the production cross section of stau leptons are set from 0.31 pb to 0.04 pb for the stau lepton mass range of 60 to 300 GeV.

IX. COMBINATION OF RESULTS

In the absence of observed signal in all three analyses, the searches for a pair of CMLLPs in 1.1 fb^{-1} of Run IIa, in 5.2 fb^{-1} of Run IIb, and the search for a single CMLLP in 5.2 fb^{-1} of Run IIb integrated luminosity, we combine the results to find limits on the production cross sections of stau leptons, gaugino-like charginos, and higgsino-like charginos. Due to the effect of hadronization and charge-flipping, the sensitivity of the search for single CMLLPs for top squarks is much better than the sensitivity of the search for a pair of CMLLPs. As a result, the top squark mass limits for the combination of the single CMLLP (with a veto for the events common with the pair search) and the pair CMLLP analyses do not show a significant improvement over the results from the single CMLLP analysis on its own and hence is not performed.

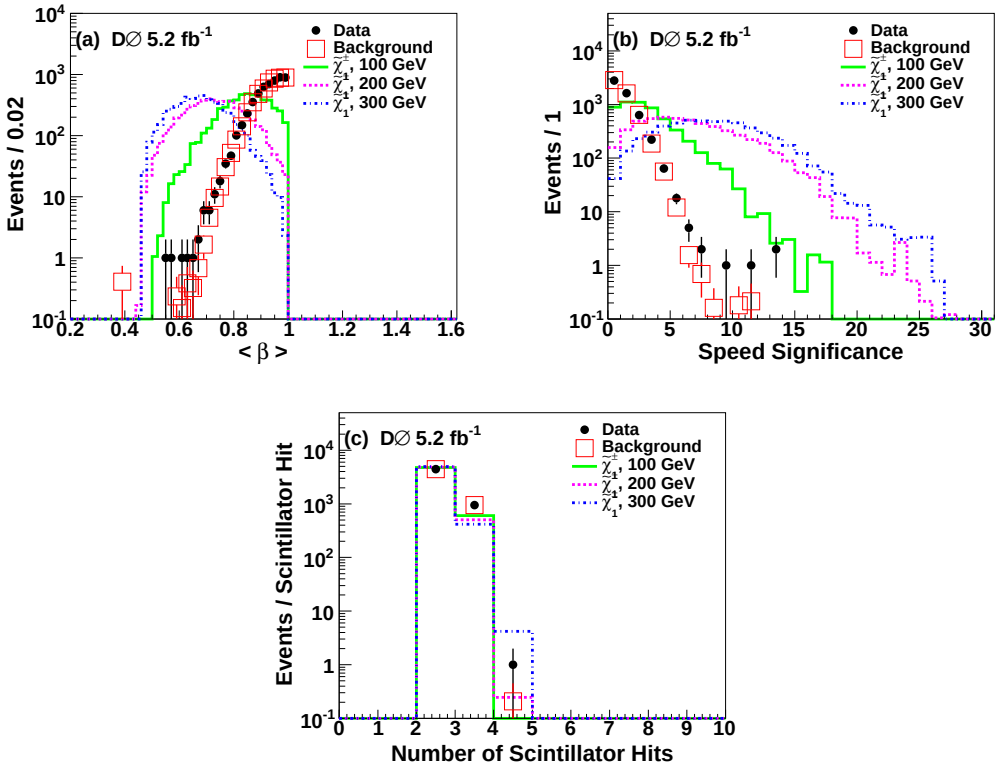

FIG. 19: (color online) Speed related input distributions to BDTs for the search for single CMLLPs. Background comes from events containing a muon with $\langle\beta\rangle < 1$ and $M_T \leq 200$ GeV. Signal is gaugino-like charginos of masses 100 GeV, 200 GeV, and 300 GeV. The distributions are normalized to the same number of events.

A. Method of Combination

In the Run IIb search for a pair of CMLLPs, the value of the requirement on the BDT output is optimized for each signal mass point. A similar procedure was used in the search for a pair of CMLLPs with Run IIa data. In the search for single CMLLPs in Run IIb, the entire BDT distribution is used as input to a CL_s limit setting method. To obtain results from the combination of the three analyses, the signal acceptance, the number of predicted background events, and the number of observed events for each signal mass, for the two pair analyses (Tables VIII, XVI) along with the BDT distributions from the search for single CMLLPs (Figs. 21, and 27-29) (see Appendix A) are used as inputs to the same CL_s method. To avoid double counting of events, the datasets used for the two Run IIb analyses are made statistically independent by removing the events that have been selected for the search of CMLLP pairs from the dataset used to search for single CMLLPs. The different analyses are combined by summing the log-likelihood ratios over all the bins and all the analyses.

B. Systematic Uncertainties

Systematic uncertainties are treated as Gaussian distributions and are applied to the expected number of signal and background events. Various sources of systematic uncertainties along with their values for the four types of CMLLP signals that have been studied are listed in Table XVII and the systematic uncertainties on the background sample are listed in Table XVIII. All systematic uncertainties except the luminosity uncertainty [33] for the two searches for pairs of CMLLPs are treated as uncorrelated. The recent search for CMLLP pairs and the search for a single CMLLP are based on the same dataset. Therefore, the systematic uncertainties for these two analyses are correlated except for the uncertainties on background normalizations (the background samples are different in the two analyses). The systematic uncertainties for the single CMLLP dataset after removal of the events containing CMLLP pairs are the same as those in the search for a single CMLLP analysis described in Sec. VII D. The shape systematic uncertainties however are updated after the removal of the common events.

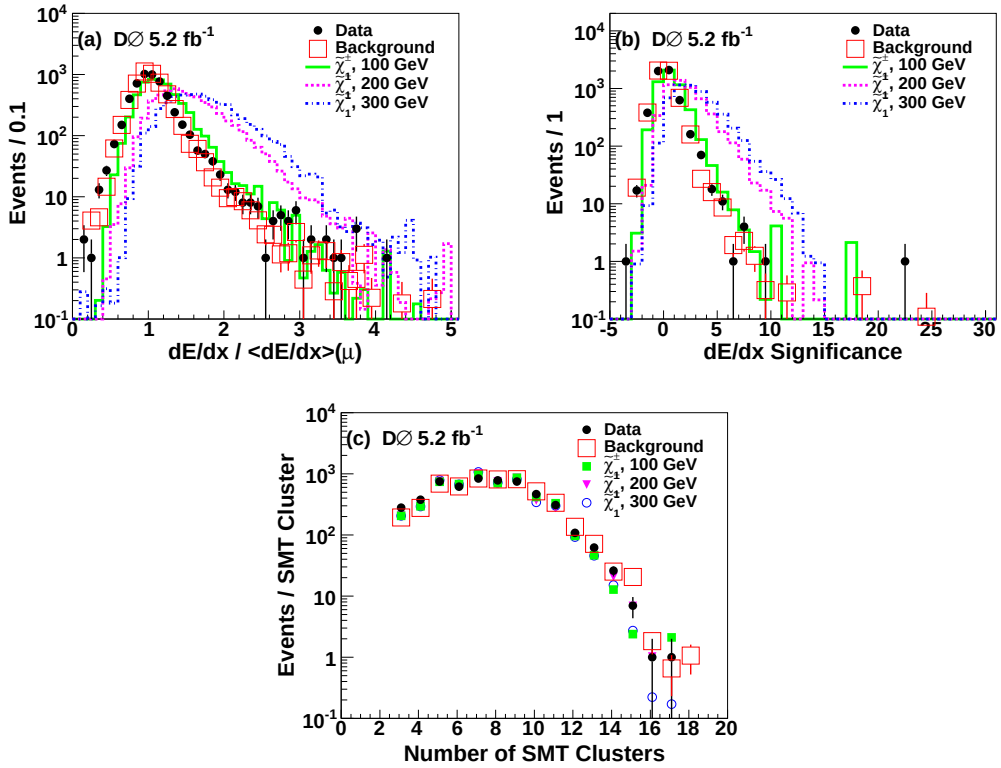

FIG. 20: (color online) Distributions related to $\mathrm{d}E/\mathrm{d}x$ used in the BDT for the search for single CMLLPs. Background comes from events containing a muon with $\langle\beta\rangle < 1$ and $M_T \leq 200$ GeV. Signal is gaugino-like charginos of masses 100 GeV, 200 GeV, and 300 GeV. The distributions are normalized to the same number of events.

C. Results

Combined 95% C.L. cross section limits for stau leptons, gaugino-like, and higgsino-like charginos are shown in Table XIX, and Fig. 23. Using the observed cross section and the theoretical NLO cross section, we set mass limits of 278 GeV for gaugino-like charginos and 244 GeV for higgsino-like charginos. Using the intersection of the -1 $(+1)$ standard deviation (σ) band on the NLO cross section shifts the mass limits down (up) by $\sim$1 GeV for the charginos. We do not have enough sensitivity to set a limit on the stau lepton mass and therefore we set an upper limit on production cross sections of stau leptons to be 0.04 pb to 0.008 pb for the stau lepton mass range of 100 to 300 GeV.

X. SUMMARY

A search for CMLLPs has been performed with the D0 detector with 5.2 fb^{-1} integrated luminosity using two different strategies: a search for a pair of identified CMLLPs and a search for a single identified CMLLP in events expected to contain a pair of CMLLP's. These two searches are combined with the earlier search for CMLLP pairs with 1.1 fb^{-1} integrated luminosity. We use the central value of the theoretical cross section predictions to set 95% C.L. lower limits on the masses of top squarks and charginos and on the cross section of stau leptons.

Using the combination of the three searches we set mass limits of 278 GeV for gaugino-like charginos and 244 GeV for higgsino-like charginos. For stau leptons we set an upper limit of 0.04 pb to 0.008 pb on the production cross section for the mass range of 100 to 300 GeV.

In the search for single CMLLPs we exclude top squarks with masses below 285 GeV with a charge flipping probability of 38%. A combination of the analyses is not performed for the top squarks since improvement in the stop limit by combining the searches is negligible.

Limits on the chargino cross sections are the most restrictive limits to date, with about an order of magnitude improvement over the previous D0 result with 1.1 fb^{-1} integrated luminosity [5]. The improvement in both the pair and the single CMLLP searches over the previous results is due to the increased luminosity as well as the additional use of another key variable, the measured $\mathrm{d}E/\mathrm{d}x$ of the tracks.

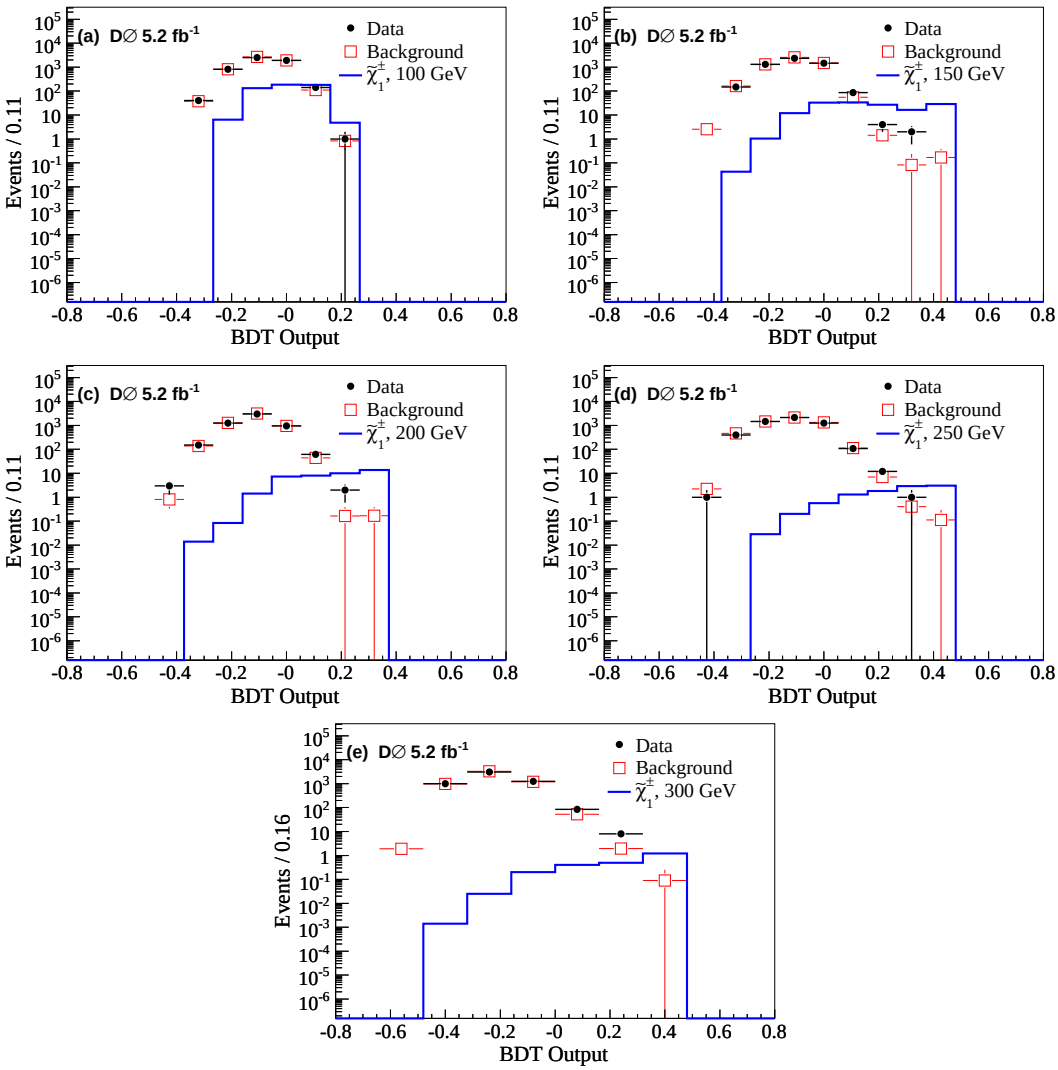

FIG. 21: (color online) BDT-output distributions for simulated gaugino-like chargino masses 100–300 GeV in 50 GeV steps in the search for single CMLLPs. The distributions are normalized to the expected number of events.

Acknowledgments

We thank the staffs at Fermilab and collaborating institutions, and acknowledge support from the DOE and NSF (USA); CEA and CNRS/IN2P3 (France); MON, Rosatom and RFBR (Russia); CNPq, FAPERJ, FAPESP and FUNDUNESP (Brazil); DAE and DST (India); Colciencias (Colombia); CONACyT (Mexico); NRF (Korea); FOM (The Netherlands); STFC and the Royal Society (United Kingdom); MSMT and GACR (Czech Republic); BMBF and DFG (Germany); SFI (Ireland); The Swedish Research Council (Sweden); and CAS and CNSF (China).

[1] M. Byrne, C. Kolda, and P. Regan, Phys. Rev. D **66**, 075007 (2002).

[2] K. Nakamura *et al.* (Particle Data Group), J. Phys. G **37**, 075021 (2010), see *Big Bang Nucleosynthesis (rev.)*, Section 20.5 and references cited therein.

[3] M. Eads, Ph.D. Thesis, Northern Illinois University, FERMILAB-THESIS-2005-24 (2004).

[4] Y. Xie, Ph.D. Thesis, Brown University, FERMILAB-THESIS-2009-37 (2009).

[5] V. Abazov *et al.* (D0 Collaboration), Phys. Rev. Lett. **102**, 161802 (2009).

[6] D. Acosta *et al.* (CDF Collaboration), Phys. Rev. Lett. **90**, 131801 (2003).

[7] T. Aaltonen *et al.* (CDF Collaboration), Phys. Rev. Lett.

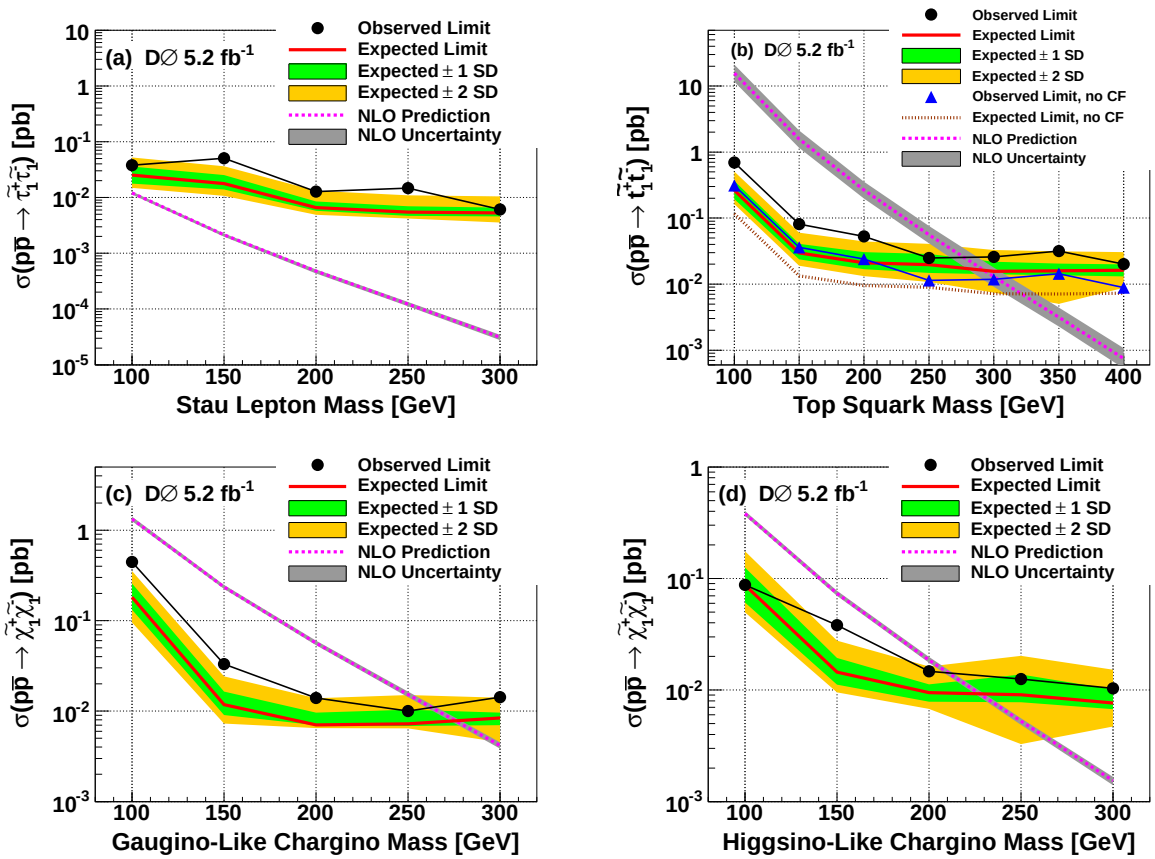

FIG. 22: (color online) 95% C.L. limits on production cross sections of a pair of stau leptons, top squarks, gaugino-like charginos, and higgsino-like charginos, as a function of their masses from the search for one or more CMLLPs with Run IIb data. ±1 SD and ±2 SD are the 1 and 2 standard deviation bands respectively around the expected limit curves.

103, 021802 (2009).

[8] ALEPH, DELPHI, L3, and OPAL Collaborations, Notes LEPSUSYWG/02-05.1 and LEPSUSYWG/02-09.2.

[9] V. Khachatryan *et al.* (CMS Collaboration), J. High Ener. Phys. **03**, 024 (2011).

[10] G. Aad *et al.* (ATLAS Collaboration) Phys. Lett. B **698**, 353 (2011).

[11] V. Abazov *et al.* (D0 Collaboration), Phys. Rev. Lett. **108**, 121802 (2012).

[12] P. Smith *et al.*, Nucl. Phys. B **206**, 333 (1982).

[13] M. Dine and A. E. Nelson, Phys. Rev D **48**, 1277 (1993).

[14] M. Dine, A. E. Nelson, Y. Nir, and Y. Shirman, Phys. Rev. D **53**, 2658 (1996).

[15] J. Feng and T. Moroi, Phys. Rev. D **58**, 035001 (1998).

[16] S. Martin, hep-ph/9709356 (1997).

[17] J. Feng, S. Su, and F. Takayama, Phys. Rev. D **70**, 063514 (2004).

[18] J. Feng, S. Su, and F. Takayama, Phys. Rev. D **70**, 075019 (2004).

[19] J. Gunion and S. Mrenna, Phys. Rev. D **62**, 015002 (2000).

[20] C. Chen, M. Drees, and J. Gunion, Phys. Rev. D **55**, 330 (1997).

[21] G. F. Giudice and A. Rattazzi, Phys. Rept. **322**, 419 (1999).

[22] M. J. Strassler, hep-ph/0607160 (2006).

[23] M. J. Strassler and K. M. Zurek, hep-ph/0604261 (2006).

[24] V. M. Abazov, *et al.* (D0 Collaboration), Nucl. Instrum. Methods Phys. Res., A **565**, 463 (2006); M. Weber *et al.*, Nucl. Instrum. Methods Phys. Res. A **566**, 182 (2006); M. Abolins *et al.*, Nucl. Instrum. Methods Phys. Res. A **584**, 75 (2007).

[25] V. M. Abazov, *et al.* (D0 Collaboration), Nucl. Instrum. Methods Phys. Res. A **552**, 372 (2005).

[26] T. Sjostrand, S. Mrenna and P. Skands, J. High Energy Phys. **605**, 026 (2006). We use PYTHIA 6.409.

[27] S. P. Martin, S. Moretti, J. Qian, and G. W. Wilson, in *Proceedings of APS/DPF/DPB Summer Study on the Future of Particle Physics*, eConf C010630, P346 (2001). See also model SPS7 in B. C. Allanach *et al.*, Eur. Phys. J. C **25**, 113 (2002).

[28] The code for generating top squarks is available at http://projects.hepforge.org/pythia6/examples/main78.f

[29] R. Brun et al., CERN Program Library Long Writeup W5013 (1993).

[30] B.C. Allanach, Comput. Phys. Commun. **143**, 305 (2002).

[31] W. Beenakker, M. Klasen, M. Kramer, T. Plehn, M. Spira and P. M. Zerwas, Phys. Rev. Lett. **8**, 3780 (1999).

[32] K. Nakamura *et al.* (Particle Data Group), *ibid.*, see *Pas-*

Mass (GeV)	NLO cross section [pb]	σ_{95}^{obs} [pb]	σ_{95}^{exp} [pb]
Stau lepton			
100	$0.0120^{+0.0006}_{-0.0008}$	0.038	$0.025^{+0.011}_{-0.0075}$
150	$0.0021^{+0.0001}_{-0.0002}$	0.050	$0.018^{+0.0076}_{-0.0038}$
200	$0.00050^{+0.00003}_{-0.00002}$	0.013	$0.0066^{+0.0020}_{-0.0008}$
250	$0.00010^{+0.00001}_{-0.00001}$	0.015	$0.0055^{+0.0015}_{-0.0008}$
300	$0.000030^{+0.000003}_{-0.000004}$	0.006	$0.0053^{+0.0013}_{-0.0007}$
Top squark			
100	$15.6^{+5.4}_{-4.0}$	0.70	$0.26^{+0.094}_{-0.078}$
150	$1.58^{+0.53}_{-0.42}$	0.081	$0.030^{+0.011}_{-0.0063}$
200	$0.27^{+0.088}_{-0.068}$	0.053	$0.021^{+0.0096}_{-0.0043}$
250	$0.056^{+0.020}_{-0.014}$	0.025	$0.020^{+0.0088}_{-0.0049}$
300	$0.013^{+0.0048}_{-0.0039}$	0.026	$0.016^{+0.0061}_{-0.0016}$
350	$0.0032^{+0.0012}_{-0.0009}$	0.032	$0.016^{+0.0046}_{-0.0024}$
400	$0.0008^{+0.0003}_{-0.0002}$	0.020	$0.016^{+0.0036}_{-0.0031}$
Gaugino-like chargino			
100	$1.33^{+0.08}_{-0.07}$	0.44	$0.180^{+0.076}_{-0.051}$
150	$0.240^{+0.014}_{-0.010}$	0.033	$0.0120^{+0.0047}_{-0.0028}$
200	$0.0570^{+0.0034}_{-0.0030}$	0.014	$0.0070^{+0.0026}_{-0.00006}$
250	$0.0150^{+0.0011}_{-0.0010}$	0.010	$0.0072^{+0.0031}_{-0.0004}$
300	$0.0042^{+0.0004}_{-0.0003}$	0.014	$0.0084^{+0.0012}_{-0.0014}$
Higgsino-like chargino			
100	$0.380^{+0.023}_{-0.017}$	0.088	$0.087^{+0.038}_{-0.026}$
150	$0.0740^{+0.0040}_{-0.0038}$	0.038	$0.015^{+0.0049}_{-0.0033}$
200	$0.0190^{+0.0012}_{-0.0010}$	0.015	$0.0095^{+0.0018}_{-0.0017}$
250	$0.0053^{+0.0004}_{-0.0004}$	0.013	$0.0091^{+0.0047}_{-0.0013}$
300	$0.0015^{+0.0001}_{-0.0001}$	0.010	$0.0077^{+0.0025}_{-0.0009}$

TABLE XV: 95% C.L. cross section limits for stau lepton, top squark, gaugino-like, and higgsino-like charginos in the search for single CMLLPs in Run IIb data.

sage of particle through matter (rev.), Section 27.2 and references cited therein.
[33] T. Andeen *et al.*, FERMILAB-TM-2365 (2007).
[34] M. Fairbairn *et al.*, Phys. Rept. **438**, 1 (2007), Table 3, page 40.
[35] R. Mackeprang and A. Rizzi, Eur. Phys. J. C**50**, 353 (2007).
[36] R. Mackeprang and D. Milstead, Eur. Phys. J. C**66**, 493 (2010).
[37] R. Mackeprang, CERN-THESIS-2007-109, page 43.
[38] A. Hoecker *et al.*, PoS ACAT 040 (2007), arXiv:physics/0703039.
[39] J. Pumplin *et al.* (CTEQ Collaboration), J. High Energy Phys. **07**, 012 (2002).
[40] I. Bertram, *et al.*, FERMILAB-TM-2104 (2000).
[41] T. Junk, Nucl. Instrum. Methods Phys. Res., A **434**, 435 (1999), A. Read J. Phys. G **28**, 2693 (2002).
[42] W. Fisher, FERMILAB Report No. TM-2386-E (2007).

APPENDIX A: BDT DISTRIBUTIONS

The BDT-output distributions for stau, top squark, and higgsino-like charginos, after being normalized to the expected number of events, for the search of a pair of CMLLPs are shown in Figs. 24–26. The BDT-output distributions for stau, top squark, and higgsino-like charginos, after being normalized to the expected number of events, for the search of a single CMLLP are shown in Figs. 27–29.

Mass (GeV)	Signal Acceptance (%)	Predicted Background	Observed Data
Stau lepton			
100	$5.56 \pm 0.11 \pm 0.41$	$1.55 \pm 0.49 \pm 0.30$	1
150	$12.3 \pm 0.16 \pm 1.27$	$1.70 \pm 0.51 \pm 0.15$	1
200	$13.9 \pm 0.17 \pm 1.11$	$1.70 \pm 0.51 \pm 0.51$	1
250	$13.3 \pm 0.16 \pm 1.25$	$1.70 \pm 0.51 \pm 0.31$	1
300	$11.7 \pm 0.15 \pm 1.34$	$1.86 \pm 0.54 \pm 0.15$	2
Gaugino-like chargino			
100	$4.63 \pm 0.10 \pm 0.35$	$1.55 \pm 0.49 \pm 0.31$	1
150	$8.51 \pm 0.13 \pm 0.88$	$1.24 \pm 0.44 \pm 0.11$	1
200	$8.89 \pm 0.13 \pm 0.71$	$1.86 \pm 0.54 \pm (< 0.01)$	1
250	$7.40 \pm 0.12 \pm 0.70$	$1.70 \pm 0.51 \pm 0.31$	1
300	$5.88 \pm 0.11 \pm 0.68$	$1.70 \pm 0.51 \pm 0.14$	2
Higgsino-like chargino			
100	$4.94 \pm 0.10 \pm 0.37$	$1.55 \pm 0.49 \pm 0.31$	1
150	$8.91 \pm 0.13 \pm 0.92$	$1.39 \pm 0.46 \pm 0.13$	1
200	$9.56 \pm 0.14 \pm 0.76$	$1.86 \pm 0.54 \pm (< 0.01)$	1
250	$8.13 \pm 0.13 \pm 0.76$	$1.70 \pm 0.51 \pm 0.31$	1
300	$6.36 \pm 0.11 \pm 0.73$	$1.70 \pm 0.51 \pm 0.14$	1

TABLE XVI: The signal acceptance, number of predicted background events, and the number of observed events from the search for a pair of CMLLPs with 1.1 fb^{-1} of Run IIa integrated luminosity. The first error is statistical and the second one is systematic.

Pair (1.1 fb^{-1})	Pair (5.2 fb^{-1})	Single (5.2 fb^{-1})
Luminosity (±6.1%)	Luminosity (±6.1%)	Luminosity (±6.1%)
Muon Reco. (±0.7%)	Muon Reco. (±2.1%)	Muon Reco. (±2.1%)
PDF (±0.1–2.7%)	PDF (±0.2%)	PDF (±0.2%)
Timing gate (±2.8–13%)	p_T resolution (±2.8%)	p_T resolution (±0.2%)
Time simulation (±6–13%)	Timing gate (±2.4%)	Timing gate (shape)
	Time simulation (±2.8%)	Time simulation (shape)
	$\mathrm{d}E/\mathrm{d}x$ corr. (±0.1%)	$\mathrm{d}E/\mathrm{d}x$ corr. (±0.02%)
	$\mathrm{d}E/\mathrm{d}x$ smearing (±0.6%)	$\mathrm{d}E/\mathrm{d}x$ smearing (±0.2%)
	MDT Timing gate (±1.2%)	Speed χ^2/dof Corr. (±0.4%)
	Speed Asym. Corr. (±1.06–10.1%)	

TABLE XVII: Systematic uncertainties for signals for all three analyses.

Pair (1.1 fb^{-1})	Pair (5.2 fb^{-1})	Single (5.2 fb^{-1})
Bkgd. Norm. (±9-28%)	Luminosity (±6.1%)	dE/dx Corr. Uncertainty (±0.02)
	Muon Reco. (±2.1%)	Bkgd. Norm.-$\langle\beta\rangle$ (±7.2%)
	PDF (±0.3%)	Bkgd. Norm.-M_T (±2.2%)
	p_T resolution (±11.0%)	
	Timing gate (±3.8%)	
	Time simulation (±9.5%)	
	dE/dx Corr. (±1.5%)	
	dE/dx smearing (±4.9%)	
	Bkgd. Norm. (±2.2%)	
	Speed Asym. Corr. (±3.6%)	

TABLE XVIII: Systematic uncertainties for background events for all three analyses.

Mass (GeV)	NLO cross section (pb)	σ_{95}^{obs} (pb)	σ_{95}^{exp} (pb)
Stau lepton			
100	$0.0120^{+0.0006}_{-0.0008}$	0.041	$0.024^{+0.013}_{-0.006}$
150	$0.0021^{+0.0001}_{-0.0002}$	0.023	$0.011^{+0.004}_{-0.003}$
200	$0.00050^{+0.00003}_{-0.00002}$	0.013	$0.008^{+0.003}_{-0.001}$
250	$0.00010^{+0.00001}_{-0.00001}$	0.017	$0.008^{+0.004}_{-0.001}$
300	$0.000030^{+0.000003}_{-0.000004}$	0.008	$0.006^{+0.003}_{-0.002}$
Gaugino-like chargino			
100	$1.33^{+0.08}_{-0.07}$	0.023	$0.028^{+0.008}_{-0.010}$
150	$0.240^{+0.014}_{-0.010}$	0.013	$0.011^{+0.004}_{-0.001}$
200	$0.0570^{+0.0034}_{-0.0030}$	0.009	$0.010^{+0.003}_{-0.002}$
250	$0.0150^{+0.0011}_{-0.0010}$	0.009	$0.008^{+0.003}_{-0.001}$
300	$0.0042^{+0.0004}_{-0.0003}$	0.009	$0.009^{+0.002}_{-0.001}$
Higgsino-like chargino			
100	$0.380^{+0.023}_{-0.017}$	0.026	$0.028^{+0.014}_{-0.009}$
150	$0.074^{+0.0040}_{-0.0038}$	0.011	$0.011^{+0.005}_{-0.003}$
200	$0.0190^{+0.0012}_{-0.0010}$	0.010	$0.008^{+0.003}_{-0.002}$
250	$0.00530^{+0.00035}_{-0.0004}$	0.007	$0.008^{+0.002}_{-0.001}$
300	$0.0015^{+0.0001}_{-0.0001}$	0.011	$0.009^{+0.001}_{-0.001}$

TABLE XIX: Combined 95% C.L. cross section limits for stau leptons, gaugino-like, and higgsino-like charginos from the three search strategies.

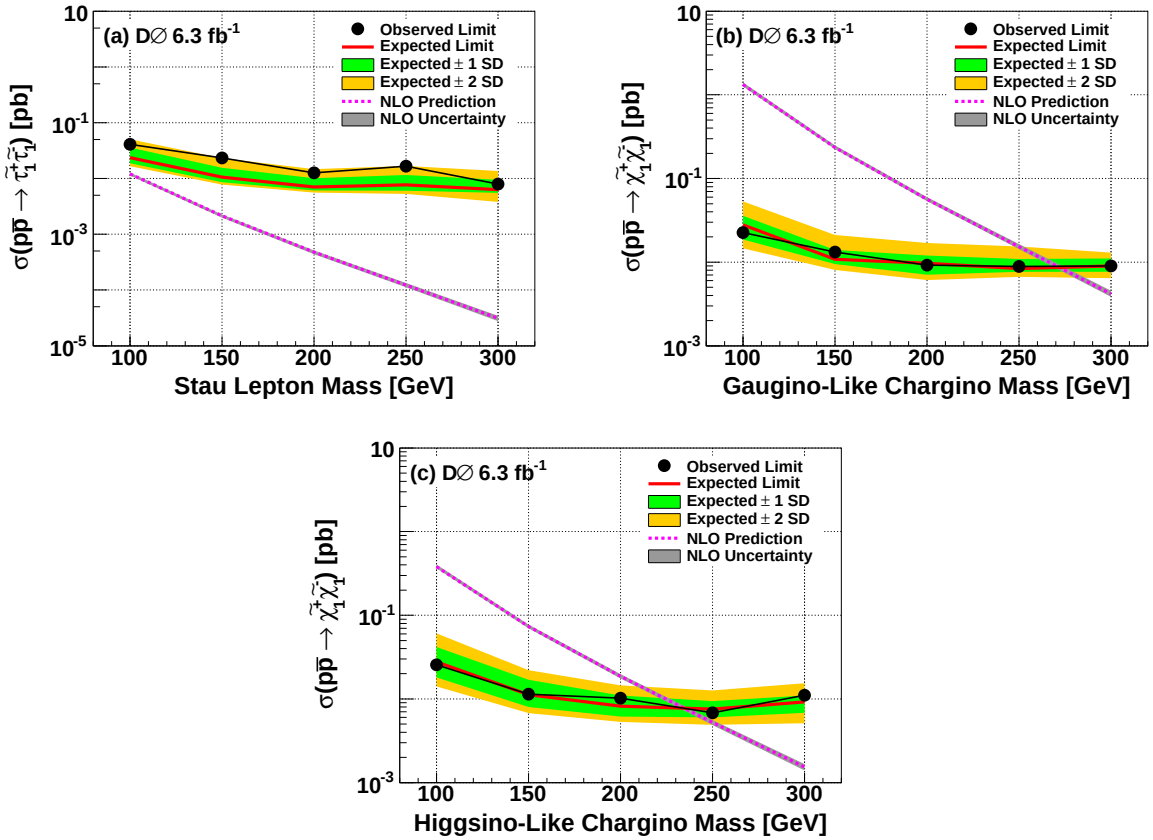

FIG. 23: (color online) Combined limits at 95% C.L. on production cross sections of a pair of stau leptons, gaugino-like charginos, and higgsino-like charginos as a function of their masses with Run IIa and Run IIb data. ±1 SD and ±2 SD are the 1 and 2 standard deviation bands respectively around the expected limit curves.

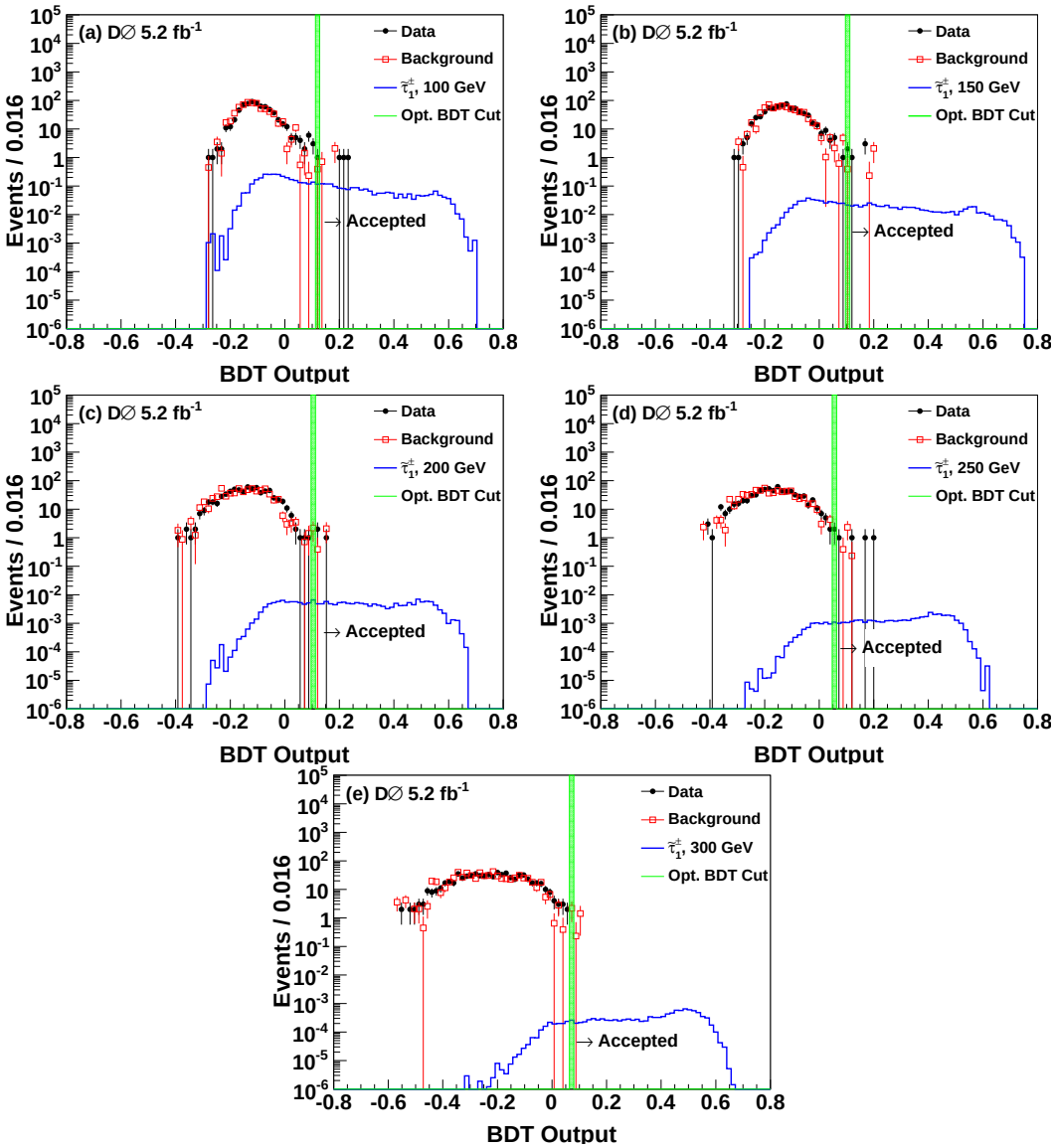

FIG. 24: (color online) BDT-output distributions for stau masses 100-300 GeV in 50 GeV steps for the search for a CMLLP pair with Run IIb data. The distributions are normalized to the expected number of events. The selection requirement on the BDT value is shown with a green vertical line.

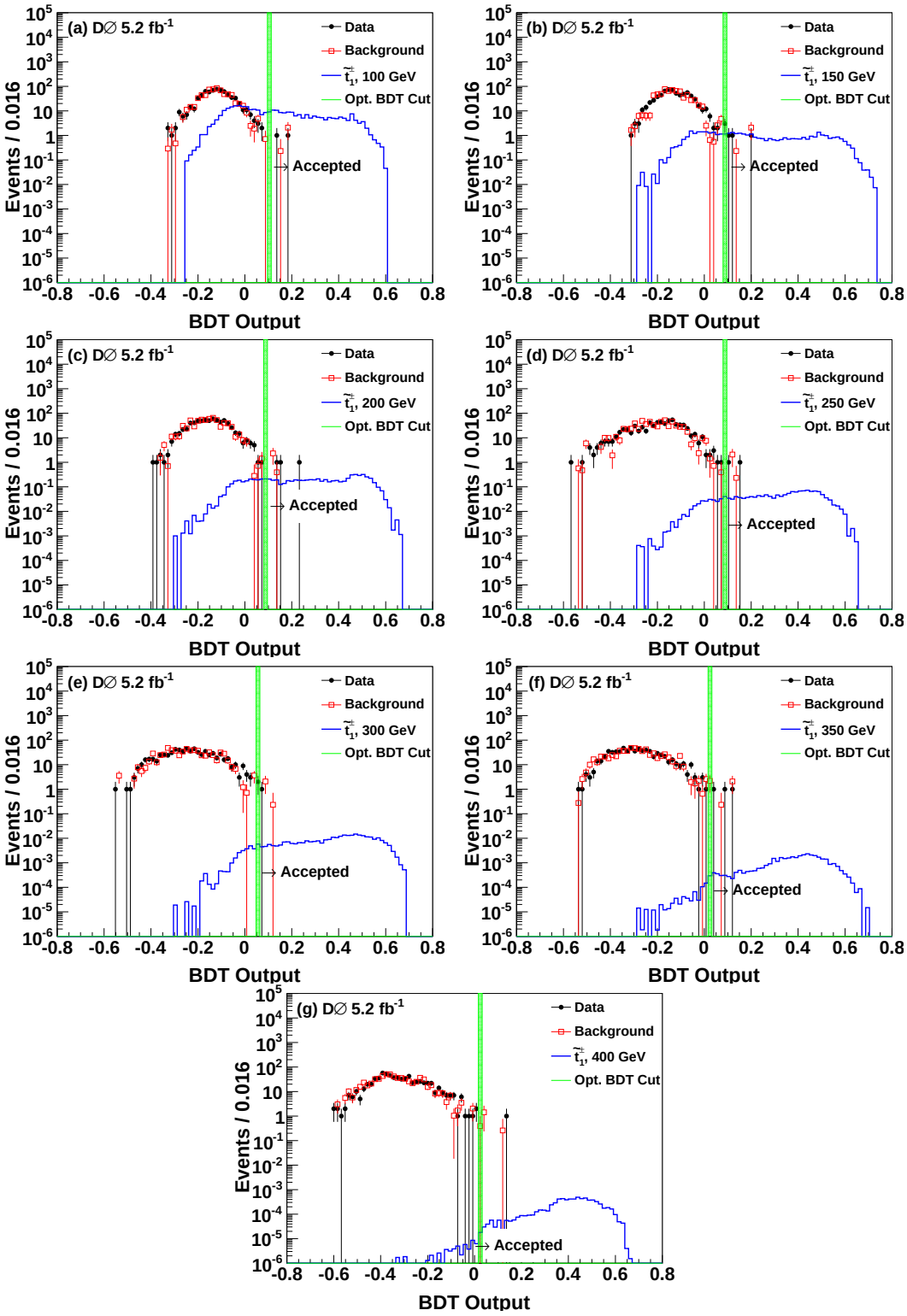

FIG. 25: (color online) BDT-output distributions for top squark masses 100-400 GeV in 50 GeV steps for the search for a CMLLP pair with the Run IIb data. Distributions are normalized to the expected number of events. Selection requirement on the BDT value is shown with a green vertical line.

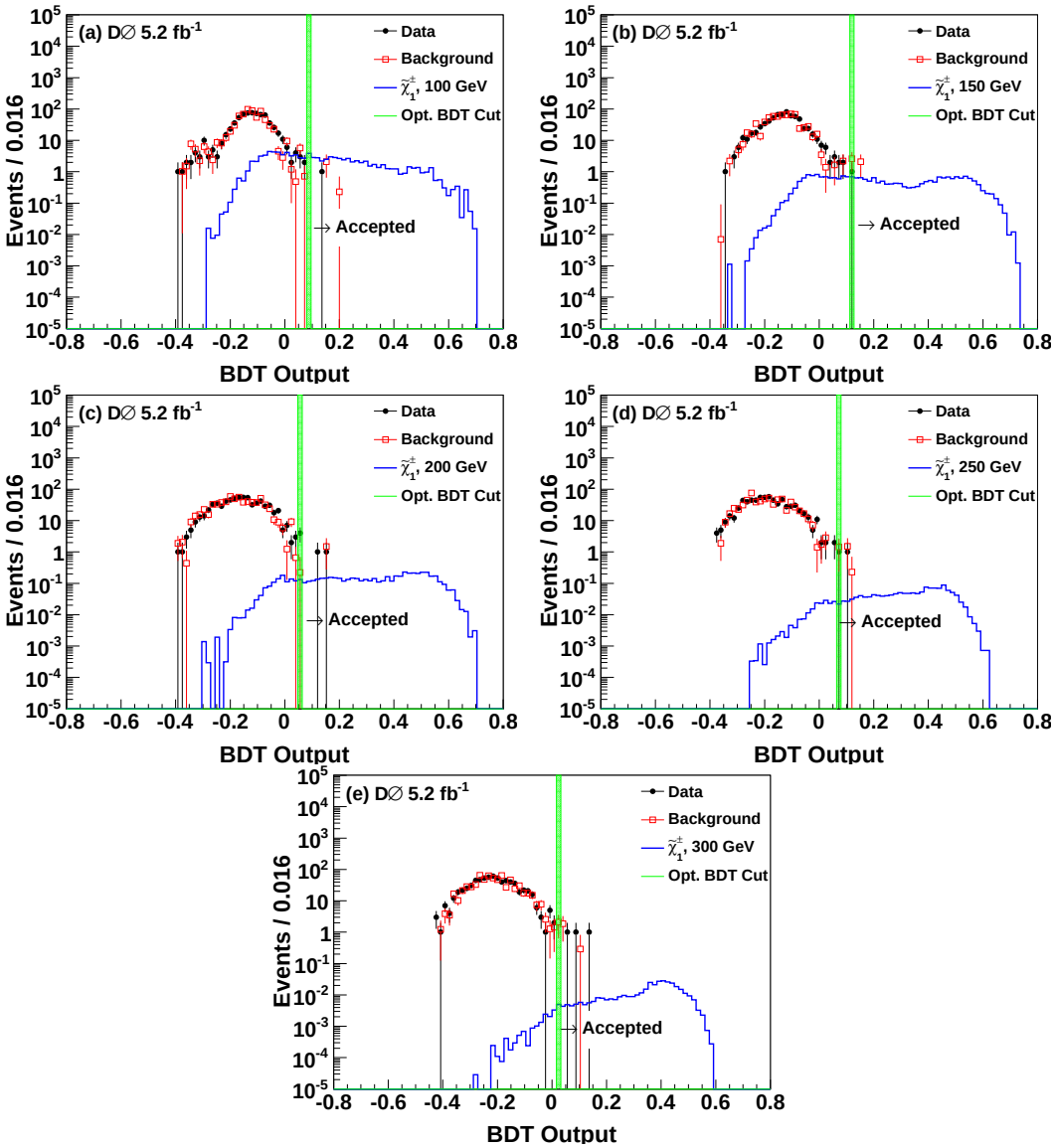

FIG. 26: (color online) BDT-output distributions for higgsino-like chargino masses 100-300 GeV in 50 GeV steps for the search for a CMLLP pair with the Run IIb data. Distributions are normalized to the expected number of events. Selection requirement on the BDT is shown with a green vertical line.

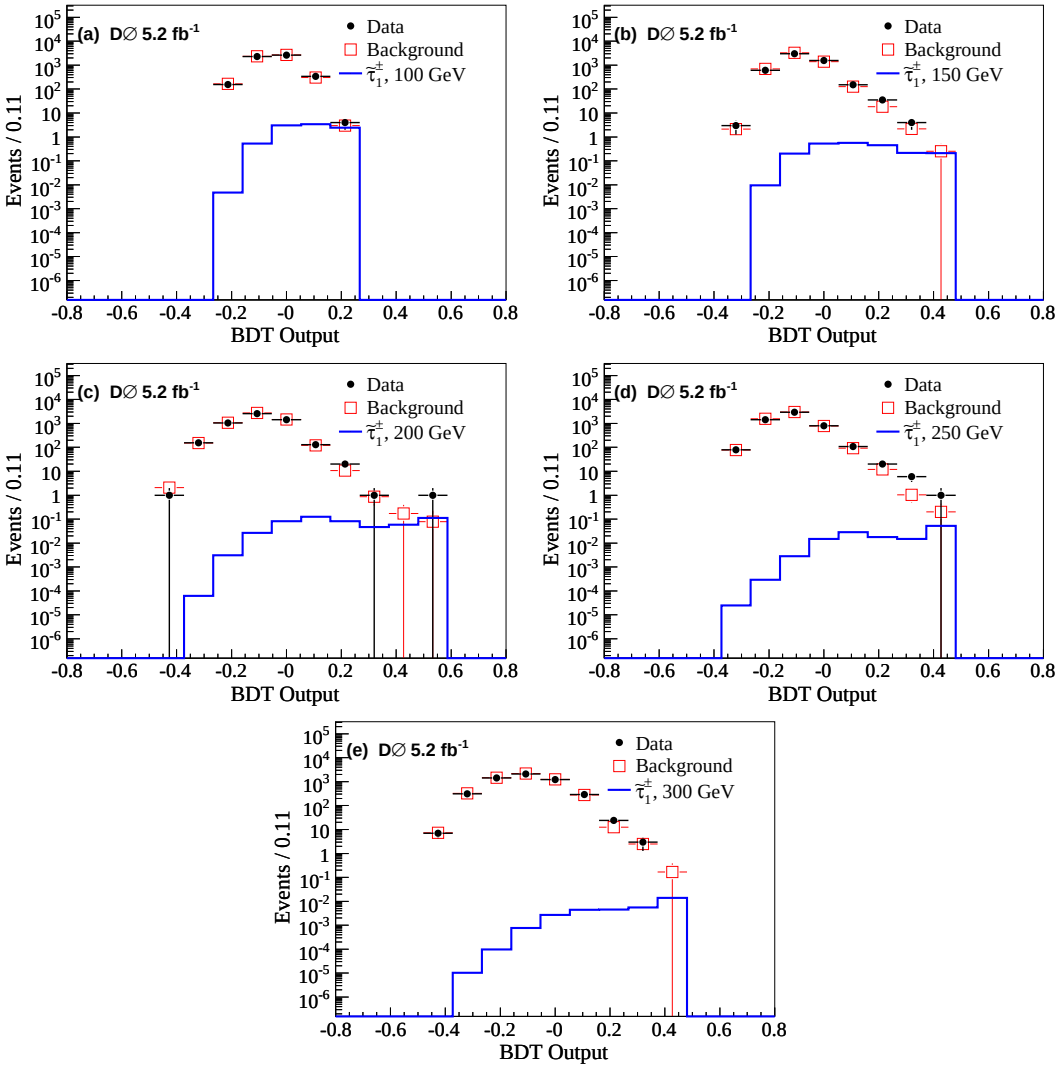

FIG. 27: (color online) BDT-output distributions for stau masses 100-300 GeV in 50 GeV steps in the search for single CMLLPs. The distributions are normalized to the expected number of events.

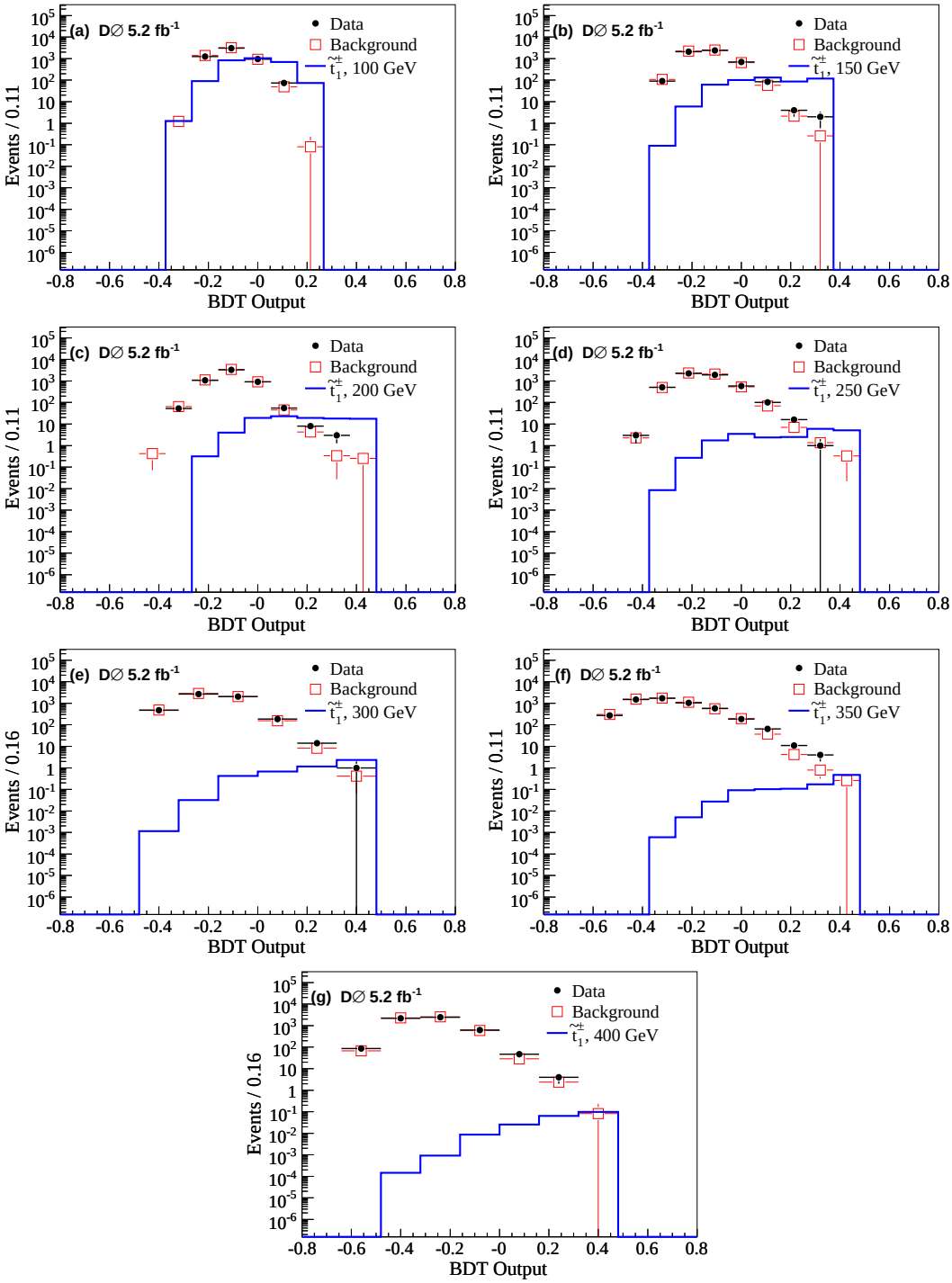

FIG. 28: (color online) BDT-output distributions for top squark masses 100-400 GeV in 50 GeV steps in the search for single CMLLPs. The distributions are normalized to the expected number of events.

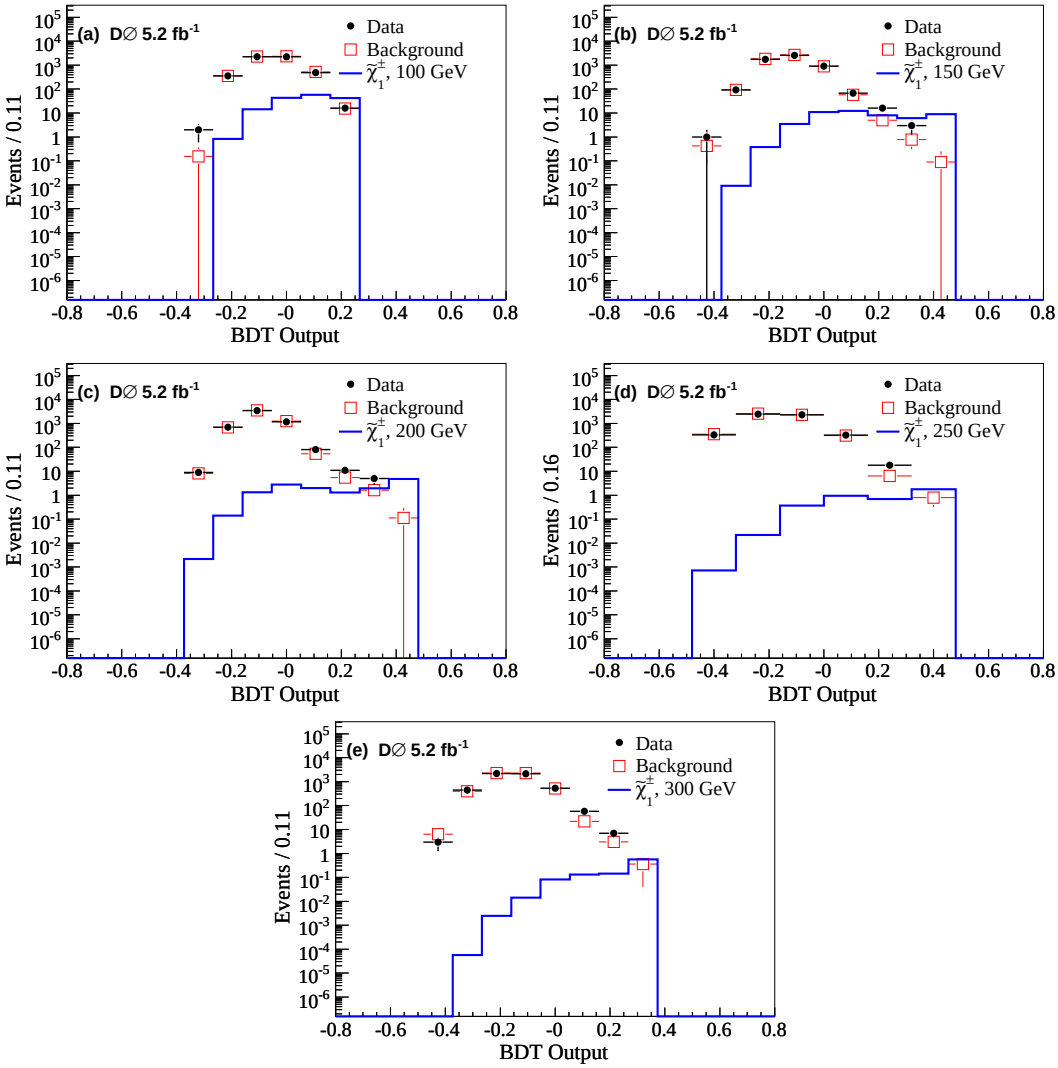

FIG. 29: (color online) BDT-output distributions for higgsino-like chargino masses 100-300 GeV in 50 GeV steps in the search for single CMLLPs. The distributions are normalized to the expected number of events.